

## Considerations for Photochemical Modeling of Possible Hycean Worlds

G. J. COOKE <sup>1,\*</sup> AND N. MADHUSUDHAN <sup>1,†</sup>

<sup>1</sup>*Institute of Astronomy, University of Cambridge, Cambridge, CB3 0HA, UK.*

### ABSTRACT

JWST is revolutionising the study of temperate sub-Neptunes, starting with the first detection of carbon-bearing molecules in the habitable-zone sub-Neptune K2-18 b. The retrieved abundances of CH<sub>4</sub> and CO<sub>2</sub> and non-detection of NH<sub>3</sub> and CO in K2-18 b are consistent with prior predictions of photochemical models for a Hycean world with a habitable ocean. However, recent photochemical modeling raised the prospect that the observed abundances may be explained by a mini-Neptune scenario instead. In this study, we explore these scenarios using independent photochemical modeling with K2-18 b as a case study. We find the previous results to be sensitive to a range of model assumptions, such as the photochemical cross sections, incident stellar spectrum, surface pressure, UV albedo, and metallicity, significantly affecting the resulting abundances. We explore a wide model space to investigate scenarios that are compatible with the retrieved molecular abundances for K2-18 b. Our analysis shows that the previously favoured mini-Neptune scenario is not compatible with most of the retrieved abundances, while the Hycean scenarios, both inhabited and uninhabited, provide better agreement. An uninhabited Hycean scenario explains most of the abundance constraints, except CH<sub>4</sub> which is generally underabundant but dependent on the model assumptions. The inhabited Hycean scenario is compatible with all the abundances if the observed CH<sub>4</sub> is assumed to be predominantly biogenic. Our results underscore the importance of systematic photochemical modeling and accurate interpretation of chemical abundance constraints for candidate Hycean worlds.

*Keywords:* Exoplanets (498) — Exoplanet atmospheres (487) — Habitable planets (695) — Exoplanet atmospheric composition (2021) — Biosignatures (2018) — Mini Neptunes(1063)

### 1. INTRODUCTION

The search for potentially habitable exoplanets and exploring their diversity is a major goal of modern astronomy. The sub-Neptune regime consists of exoplanets with radii between those of Earth and Neptune ( $\sim 1-4 R_{\oplus}$ ). These exoplanets may straddle either side of the radius valley (Fulton et al. 2017; Fulton & Petigura 2018) and have been given distinct classifications as super-Earths or mini-Neptunes depending on their size and density (Fulton & Petigura 2018; Luque & Pallé 2022; Lichtenberg & Miguel 2024). In the sub-Neptune regime, exoplanets of a certain size can be degenerate between rocky worlds that have large hydrogen-dominated atmospheres, or lower density worlds such as mini-Neptunes or water worlds, with thinner atmo-

spheres (Madhusudhan et al. 2020; Nixon & Madhusudhan 2021; Madhusudhan et al. 2023a).

In the last few years, the possibility of Hycean exoplanets has been proposed (Madhusudhan et al. 2021). These planets, with radii between  $1.1 - 2.6 R_{\oplus}$  and masses between  $1 - 10 M_{\oplus}$ , offer unique opportunities for studying their atmospheric and internal structures. Hycean exoplanets are expected to have temperature and pressure conditions that enable a liquid water ocean to exist underneath a hydrogen-rich atmosphere, with a thick layer of ice below a deep ocean (Madhusudhan et al. 2021; Rigby & Madhusudhan 2024). Given their larger radii than rocky exoplanets and the low mean molecular weight of their H<sub>2</sub>-rich atmospheres, Hycean worlds are favourable targets in the search for habitable environments beyond Earth. Promisingly, the theoretical Hycean habitable zone (Madhusudhan et al. 2021) is much larger than the purported terrestrial habitable zone (Kasting et al. 1993; Abe et al. 2011; Kopparapu

\* E-mail: gjc53@cam.ac.uk

† E-mail: nmadhu@ast.cam.ac.uk

et al. 2013, 2016; Windsor et al. 2024). On top of this, Hycean exoplanets could provide the necessary resources for life to survive and flourish, including bio-essential elements and adequate energy sources (Madhusudhan et al. 2023a).

The James Webb Space Telescope (JWST) has brought in unprecedented capability in the characterisation of temperate sub-Neptunes, demonstrated by the first detection of carbon-based molecules in the candidate Hycean world K2-18 b (Madhusudhan et al. 2023b). A transmission spectrum of K2-18 b was observed in the 1-5  $\mu\text{m}$  range (Cycle 1 GO Program 2722) which revealed a  $\text{H}_2$ -dominated atmosphere with abundances of  $\text{CH}_4$  and  $\text{CO}_2$  of  $\sim 1\%$  by volume (Madhusudhan et al. 2023b). This was the first time carbon-bearing molecules were found in a habitable zone exoplanet. Madhusudhan et al. (2023b) did not find evidence for the presence of  $\text{H}_2\text{O}$  or  $\text{NH}_3$ , which could indicate that  $\text{NH}_3$  may have been photodissociated and/or dissolved in a liquid water ocean (Hu et al. 2021; Tsai et al. 2021a; Madhusudhan et al. 2023a).

The exoplanet K2-18 b provides a valuable opportunity for atmospheric characterisation in the temperate sub-Neptune regime. The planetary parameters are shown in Table 1. The planetary bulk parameters place K2-18 b in the sub-Neptune regime with multiple solutions for the possible internal structure, including a mini-Neptune, gas dwarf, or a Hycean world (Madhusudhan et al. 2020). The instellation received by K2-18 b is very similar to that of Earth, with an equilibrium temperature ( $T_{\text{eq}}$ ) of  $\sim 235\text{-}280$  K for a Bond albedo between 0-0.5 assuming uniform redistribution. Several studies have used K2-18 b as a prototype to investigate atmospheric chemistry in the temperate sub-Neptune regime under different planetary conditions. Such models have spanned a wide range of conditions, including models with a solid/ocean surface and a thin  $\text{H}_2$ -rich atmosphere (Yu et al. 2021; Hu et al. 2021; Tsai et al. 2021a; Madhusudhan et al. 2023a) as well as mini-Neptunes and gas dwarfs with deep  $\text{H}_2$ -rich atmospheres that may be physically plausible (e.g. Hu 2021; Wogan et al. 2024; Rigby et al. 2024).

The JWST observations of K2-18 b are beginning to provide important insights into its possible internal structure and surface conditions (Madhusudhan et al. 2023b). The retrieved molecular abundances of  $\text{CH}_4$  and  $\text{CO}_2$  and non-detections of  $\text{NH}_3$  and  $\text{CO}$  are consistent with previous predictions for the presence of an ocean under a thin  $\text{H}_2$ -rich atmosphere (Yu et al. 2021; Hu et al. 2021; Tsai et al. 2021a; Madhusudhan et al. 2023a), i.e. a Hycean world (Madhusudhan et al. 2023b). Following the JWST observations of K2-18 b, some stud-

ies have proposed alternative scenarios to explain the observed spectrum, including a mini-Neptune (Wogan et al. 2024) or a putative magma ocean in which  $\text{NH}_3$  was suggested to dissolve (Shorttle et al. 2024). However, neither of these latter scenarios are able to simultaneously explain all the observed abundances, particularly the non-detections of  $\text{NH}_3$  and  $\text{CO}$  abundances coupled with a high  $\text{CO}_2$  abundance, as noted by Glein (2024). Furthermore, Rigby et al. (2024) found that the magma ocean model solutions proposed by Shorttle et al. (2024) were physically implausible as they violated mass balance and bulk density, besides being chemically incompatible with several of the retrieved abundance constraints. Other mini-Neptune scenarios proposed are also inconsistent with the retrieved abundances (Huang et al. 2024; Yang & Hu 2024a; Luu et al. 2024), albeit with different model assumptions; see e.g. Section 4.2.1. For example, Luu et al. (2024) do not consider atmospheric photochemistry, making any comparison with photospheric abundances unreliable.

Wogan et al. (2024), hereafter W24, stated that the retrieved composition of K2-18 b is broadly consistent with a mini-Neptune but not with an uninhabited Hycean world, while the inhabited Hycean was considered less plausible. The primary distinction between their uninhabited and inhabited Hycean scenarios was that the former is significantly depleted in  $\text{CH}_4$  whereas the latter has a biogenic source for  $\text{CH}_4$ . The potential for a biogenic source of  $\text{CH}_4$ , via methanogenesis, in K2-18 b was suggested in previous studies (Madhusudhan et al. 2023a,b). It was also shown previously that an uninhabited Hycean world with a 1 bar surface pressure, as considered by W24, results in significantly lower  $\text{CH}_4$  abundance in the atmosphere compared to one with a deeper atmosphere, e.g. 100 bar (Madhusudhan et al. 2023a). The allowed surface pressure for the uninhabited Hycean scenario depends strongly on the dayside albedo which is presently unconstrained. However, if the uninhabited Hycean scenario is indeed incompatible with the  $\text{CH}_4$  abundance and if, as noted by Glein (2024), the W24 mini-Neptune scenario is incompatible with multiple abundances, then the inhabited Hycean scenario emerges as the most viable explanation of the three, with significant implications for habitability. Therefore, it is important to conduct a detailed exploration of the three scenarios to investigate if indeed the retrieved abundances of K2-18 b can be better explained by the mini-Neptune scenario of W24 than the Hycean scenarios.

In what follows, we discuss our methods in Section 2. In Section 3 we investigate the mini-Neptune vs Hycean world scenarios for K2-18 b using the photochemical

Parameter	K2-18 b
Planetary mass [ $M_{\oplus}$ ]	8.63±1.35 [1]
Planetary radius [ $R_{\oplus}$ ]	2.610±0.087 [1]
Bulk density [ $\text{g cm}^{-3}$ ]	2.67 $^{+0.52}_{-0.47}$ [1]
Instellation [ $S_0$ ]	1.005 $^{+0.084}_{-0.079}$ [1]
Orbital period [d]	32.940045±0.000010 [1]
$\log_{10}(\text{CH}_4)$ mixing ratio	-1.74 $^{+0.59}_{-0.69}$ [2]
$\log_{10}(\text{CO}_2)$ mixing ratio	-2.09 $^{+0.51}_{-0.94}$ [2]
$\log_{10}(\text{H}_2\text{O})$ mixing ratio	< -3.06 [2]
$\log_{10}(\text{NH}_3)$ mixing ratio	< -4.51 [2]
$\log_{10}(\text{CO})$ mixing ratio	< -3.50 [2]

**Table 1.** Bulk properties and atmospheric abundances of K2-18 b. For the abundances, reported by Madhusudhan et al. (2023b), we use the retrieved constraints based on their canonical “One offset” case. References. (1) Benneke et al. (2019), (2) Madhusudhan et al. (2023b)

modeling framework of W24 and assess their results. We then conduct a more general exploration of the model parameter space using two photochemical models and our results are presented in Section 4. We summarise and discuss our conclusions in Section 5.

## 2. METHODS

In this section, we outline our modeling setup for further exploring photochemistry across the three atmospheric scenarios, using K2-18 b as a case study. We discuss the rationale for the simulations we perform, describe the different initial conditions used, and expand the simulated parameter space in order to examine the influence of additional variables on the predicted atmospheric composition for K2-18 b.

W24 performed their mini-Neptune atmospheric simulations using a combination of PICASO (Batalha et al. 2019; Robbins-Blanch et al. 2022; Mukherjee et al. 2023) and Photochem (Wogan et al. 2023, 2024). PICASO is used to establish the  $P$ - $T$  profile and initial states in chemical equilibrium in the deeper mini-Neptune atmosphere. Photochem is used for chemical kinetics and photochemistry simulations. For the two Hycean scenarios, W24 used only Photochem. We first use the same setup as W24 for all three scenarios in order to reproduce their results as described in Section 3 and shown in Fig. 1. In the same figure, we also reproduce the W24 results using VULCAN (Tsai et al. 2017, 2021b) in combination with the chemical equilibrium code FastChem (Stock et al. 2018, 2022; Kitzmann et al. 2024) for the mini-Neptune case, and using only VULCAN for the Hycean cases. We perform sensitivity tests for each scenario in Section 4.1 with their respective W24 setup. Additional model runs with VULCAN are carried out and the results are de-

scribed in Section 4.2. Before detailing the parameters we varied for the simulations, we briefly describe these models.

### 2.1. Photochem model

The Photochem<sup>1</sup> model hails from a previous photochemical model developed over several decades (e.g, Kasting et al. 1985; Segura et al. 2003), culminating in the Atmos<sup>2</sup> photochemical model (Arney et al. 2017) before being adapted into PhotochemPy (Wogan et al. 2022) and finally Photochem. The Photochem model is described in Appendix C of Wogan et al. (2023), where it was validated by comparing model outputs with observations from Earth and Titan (Wogan et al. 2023).

W24 implemented some updates to the thermodynamic data and reaction network that was published in Wogan et al. (2023). In particular, they describe the importance of the  $\text{O} + \text{H} + \text{H}$  photolysis channel which has a given branching ratio of 0.12 at 121.0 nm (near Lyman- $\alpha$ ). Inclusion of this channel changed the mixing ratio of  $\text{CH}_4$  in the Hu et al. (2021) 400 ppm- $\text{CO}_2$  model run from  $10^{-2}$  to  $3 \times 10^{-5}$ . This was evidently an important change, but we suggest more updates to the input data are required: Fig. B2 shows that large discrepancies exist in branching ratios between different open-source models. Some of the Photochem branching ratios (e.g. for  $\text{CH}_4$  and  $\text{NH}_3$ ) may not be accurate because they are constant with wavelength.

Only Photochem was used for the Hycean scenarios in W24. A climate code within the Photochem software package (which utilises correlated-k radiative transfer) was used to calculate the  $P$ - $T$  profile for the Hycean world, assuming 30% of radiation reflected at the top of the atmosphere. What resulted was a  $P$ - $T$  profile starting with a 320 K surface temperature, which then traced the moist pseudo adiabat in the lower atmosphere at pressures greater than 20 mbar, before reaching a 215 K isothermal stratosphere.

### 2.2. PICASO model

PICASO<sup>3</sup> is a Python-based 1D atmospheric radiative-convective equilibrium model which enables 1D climate modeling of hydrogen-dominated exoplanet atmospheres and associated synthetic spectroscopy. For their mini-Neptune case, W24 first performed an atmosphere simulation with PICASO to generate a pressure-temperature ( $P$ - $T$ ) profile and equilibrium mixing ratios of various molecules. They use a Photochem kinetic simu-

<sup>1</sup> <https://github.com/Nicholaswogan/photochem/tree/main>

<sup>2</sup> <https://github.com/VirtualPlanetaryLaboratory/atmos>

<sup>3</sup> <https://github.com/natashabatalha/picaso>

lation between 1 – 500 bar to compute the chemical equilibrium-to-disequilibrium transition at 1 bar, assuming lower boundary conditions based on chemical equilibrium. Then, connecting the  $P$ - $T$  profile to an isothermal atmosphere, *Photochem* was used to predict the concentrations of species between 1 bar and  $10^{-8}$  bar with photochemistry implemented. In this photochemistry simulation, the lower boundary conditions at 1 bar were fixed for species with mixing ratios greater than  $10^{-8}$  (10 ppbv) from the kinetics simulation.

### 2.3. VULCAN model

VULCAN<sup>4</sup> is a photochemical kinetics model for simulating the atmospheres of exoplanets (Tsai et al. 2017, 2021b). VULCAN can utilise the equilibrium chemistry code *FastChem*<sup>5</sup> (Stock et al. 2018, 2022; Kitzmann et al. 2024) to establish initial states in chemical equilibrium. One can initialise runs with a constant vertical mixing ratio instead, and specify fixed fluxes or mixing ratios at the lower boundary. It has recently been used to simulate the mixing ratios of sulfur biosignatures, such as dimethyl sulfide (DMS), over a range of different conditions and UV fluxes, before estimating their detectability (Tsai et al. 2024a). Unlike *Atmos* and *Photochem* which only uses one value for photochemical cross sections, VULCAN has three separate physical categories for cross sections: photoionisation, photodissociation, and photoabsorption.

### 2.4. Simulation setup

We first use the modeling setup of W24 to reproduce their results. We then also reproduce these results using VULCAN, before altering some assumptions in both models to achieve different results to W24. With each model, we perform simulations of all three scenarios: mini-Neptune, uninhabited Hycean, and inhabited Hycean.

The simulations using the W24 setup are shown in Table A1. For each scenario with the W24 setup, we vary the assumed photochemical cross sections (see Appendix B) and the stellar spectrum (see Appendix C). In the mini-Neptune setup, we additionally vary the metallicity (30 – 200× solar), the C/O ratio (0.25 – 2× solar), and the internal temperature,  $T_{\text{int}}$ , of the exoplanet (30 – 70 K).

The convergence criterion in VULCAN is defined in section 3 of Tsai et al. (2017) by equations 10 and 11. If the variation in the model is less than a given factor over

a defined period of model time, then the convergence criterion is satisfied and the model integration stops. However, VULCAN can sometimes appear to converge and conclude the run before steady state has been achieved in the model (Nick Wogan, Shami Tsai; private communication). Where necessary, we override this steady state criterion by setting  $y_{\text{conv\_cri}} = 0$  and  $y_{\text{conv\_min}} = 0$  in the file *vulcan\_cfg.py*.

The VULCAN simulations are listed in Table A2. In the mini-Neptune scenario, we perform simulations over different metallicities and compare to the W24 results. For the uninhabited Hycean scenario, we extend the surface pressure to explore the effect it has on the resultant composition. The mini-Neptune simulation converges relatively quickly compared to the Hycean scenarios. Therefore, in the Hycean cases, we ran VULCAN for a total of  $10^{17}$  s ( $\sim 3.2$  Gyr), noting here that the estimated age of K2-18 is  $2.4 \pm 0.6$  Gyr (Guinan & Engle 2019). This simulation time accounts for a conservative upper estimate of the age of the system in order to capture the possible long atmospheric lifetime of some molecules.

Initial conditions, including the abundances of chemical species and elemental ratios, can impact the final calculated concentrations of molecules. For the W24 uninhabited Hycean case, the final  $\text{CH}_4$  mixing ratio is  $3 \times 10^{-10}$ , assuming that the atmosphere starts with essentially no  $\text{CH}_4$  and accumulates it through photochemical reduction of  $\text{CO}_2$  to  $\text{CH}_4$ . However, the  $\text{H}_2$ -rich atmosphere of K2-18 b is unlikely to form with negligible amounts of  $\text{CH}_4$ , so we test different starting abundances and different initial metallicities in VULCAN for the Hycean scenarios. On Hycean exoplanets, the  $\text{CO}_2$  abundance in the atmosphere is set by ocean chemistry (Kite & Ford 2018; Hu et al. 2021), rather than initial chemical equilibrium conditions in the atmosphere. Therefore, in line with previous work (Tsai et al. 2024a) including W24, for the Hycean cases, we fix the  $\text{CO}_2$  abundance to ensure it is consistent with retrieved atmospheric abundances. For the inhabited Hycean scenarios, we vary the  $\text{CH}_4$  flux at the lower boundary (1 bar) to represent methanogenesis from methanogens and implement a fixed deposition velocity of  $1.2 \times 10^{-4}$  cm  $\text{s}^{-1}$  as used in W24 to represent acetogens consuming CO.

We also perform simulations with VULCAN to ascertain whether any mini-Neptune cases can match the retrieved constraints for K2-18 b. We assume the same properties that W24 did for K2-18 b and assume the same setup with *FastChem* and VULCAN to recreate the PICASO and *Photochem* simulation. We use *FastChem* in VULCAN in order to determine the initial chemical composition of the exoplanet’s atmosphere, based on the

<sup>4</sup> <https://github.com/exoclimate/VULCAN>

<sup>5</sup> <https://github.com/exoclimate/FastChem>

$P$ - $T$  profile and given elemental abundances relative to hydrogen, between 500 bar and 1 bar. Like W24, we perform a kinetics simulation between 500 – 1 bar until the code converged. A  $K_{zz}$  of  $10^8 \text{ cm}^{-2} \text{ s}^{-1}$  was used between 500 – 1 bar. Then, using photochemistry with no top of atmosphere albedo, we simulate until convergence between 1 bar and  $10^{-8}$  bar, with a vertically varying  $K_{zz}$  which starts at  $10^3 \text{ cm}^{-2} \text{ s}^{-1}$  at 1 bar as in W24. In the VULCAN simulations, we use the chemical networks labelled “NCHO\_photo\_network.txt” and “SNCHO\_photo\_network\_2024.txt” for the Hycean and mini-Neptune scenarios, respectively, unless otherwise specified (some sulfur species may be sequestered in the ocean on a Hycean world; Hu et al. 2021; Loftus et al. 2019; Tsai et al. 2024a).

Molecular photoabsorption, photodissociation, and photoionisation cross sections which vary with wavelength are key parts of the input data for any photochemical model. Photodissociation cross sections quantify the likelihood of a photon initiating a photochemical reaction in a particular chemical species. Accurately representing cross sections is essential for predictions regarding exoplanetary atmospheres and the transmission, reflection, or emission spectra that could be observed from afar. For 22 molecules, including  $\text{H}_2$ ,  $\text{H}_2\text{O}$ ,  $\text{CH}_4$ ,  $\text{CO}_2$ ,  $\text{CO}$ , and  $\text{NH}_3$ , the input data is different between three open-source codes: Photochem, Atmos, and VULCAN (see Appendix B for more details). Either one set is accurate, or all are inaccurate, and many of the cross section sources in Photochem and Atmos are unknown or not listed. For all three scenarios with the W24 setup, we swap in the cross section data from VULCAN and Atmos with the Photochem data to determine the effect on predicted final composition.

The host star, K2-18, does not have its UV stellar spectra measured precisely. Therefore, several previous studies use the MUSCLES<sup>6</sup> database (for MUSCLES and Mega-MUSCLES papers, see e.g., France et al. 2016; Youngblood et al. 2016; Loyd et al. 2016; Froning et al. 2019; Wilson et al. 2021). When it comes to interpreting the retrieved abundances from spectra of JWST measurements, we aim to demonstrate why this method introduces additional uncertainties (see appendix C for more details) by implementing three stellar proxies for K2-18 in all of the photochemical simulations.

### 3. K2-18 B: HYCEAN OR MINI-NEPTUNE?

As discussed above, W24 investigate the atmospheric chemistry of K2-18 b under different planetary scenar-

ios, mini-Neptune vs Hycean. The mini-Neptune case corresponds to a deep (500 bar)  $\text{H}_2$ -rich atmosphere whereas the Hycean cases consider a shallow 1-bar atmosphere overlying an ocean, leading to different atmospheric/surface conditions. In what follows, we discuss the model assumptions and conclusions of W24, reproduce their results with two different modeling frameworks, and comment on the Hycean vs mini-Neptune scenarios from their work.

#### 3.1. Comparison with Retrieved Abundances

W24 conclude that their predicted abundances for the mini-Neptune case are broadly consistent with the retrieved abundances for K2-18 b. Therefore, we first assess how the chemical abundances predicted by the photochemical models of W24 for the different scenarios compare with the retrieved abundances for K2-18 b (Madhusudhan et al. 2023b). As previously mentioned, Glein (2024) noted that the  $\text{NH}_3$  and  $\text{CO}$  mixing ratios predicted by W24 for the mini-Neptune scenario are too high compared to the retrieved abundances. We show the comparison between the predicted abundances for all three W24 planetary scenarios and the retrieved values in the top row of Fig. 1. Our reproduction of the W24 scenarios using a separate 1D photochemical code, VULCAN, is shown in the bottom row of Fig. 1.

Using the assumptions of W24, the only planetary scenario that matches all five of the retrieved chemical abundances from the best-fit case in Madhusudhan et al. (2023b) in the observable photosphere is the simulated inhabited Hycean scenario. The uninhabited Hycean scenario matches the constraints for  $\text{H}_2\text{O}$ ,  $\text{NH}_3$ , and  $\text{CO}_2$ , with  $\text{CO}$  on the borderline just above the upper limit, and  $\text{CH}_4$  several orders of magnitude too low. In the mini-Neptune scenario, only  $\text{CH}_4$  actually matches the  $1\text{-}\sigma$  constraints, with  $\text{CO}_2$  just below the  $1\text{-}\sigma$  constraint, whilst  $\text{H}_2\text{O}$ ,  $\text{NH}_3$ , and  $\text{CO}$  have greater abundances than the  $2\text{-}\sigma$  upper limits. Therefore, contrary to the claim in W24, their mini-Neptune scenario is not consistent with the retrieved abundances.

#### 3.2. Initial conditions

We now assess the initial conditions used in W24 between the three scenarios and their influence on the predicted abundances. In their Hycean simulations, W24 assume that  $\text{CH}_4$  starts at negligible abundances, and increases primarily through a biogenic methane flux from the ocean in the inhabited case or through photochemical reduction of  $\text{CO}_2$  to  $\text{CH}_4$  in the uninhabited case. For the inhabited Hycean case, the biogenic flux is a free parameter which can be tuned to match the retrieved value; therefore, its agreement with the retrievals

<sup>6</sup> <https://archive.stsci.edu/prepds/muscles/>

## Original Wogan et al. (2024) simulations

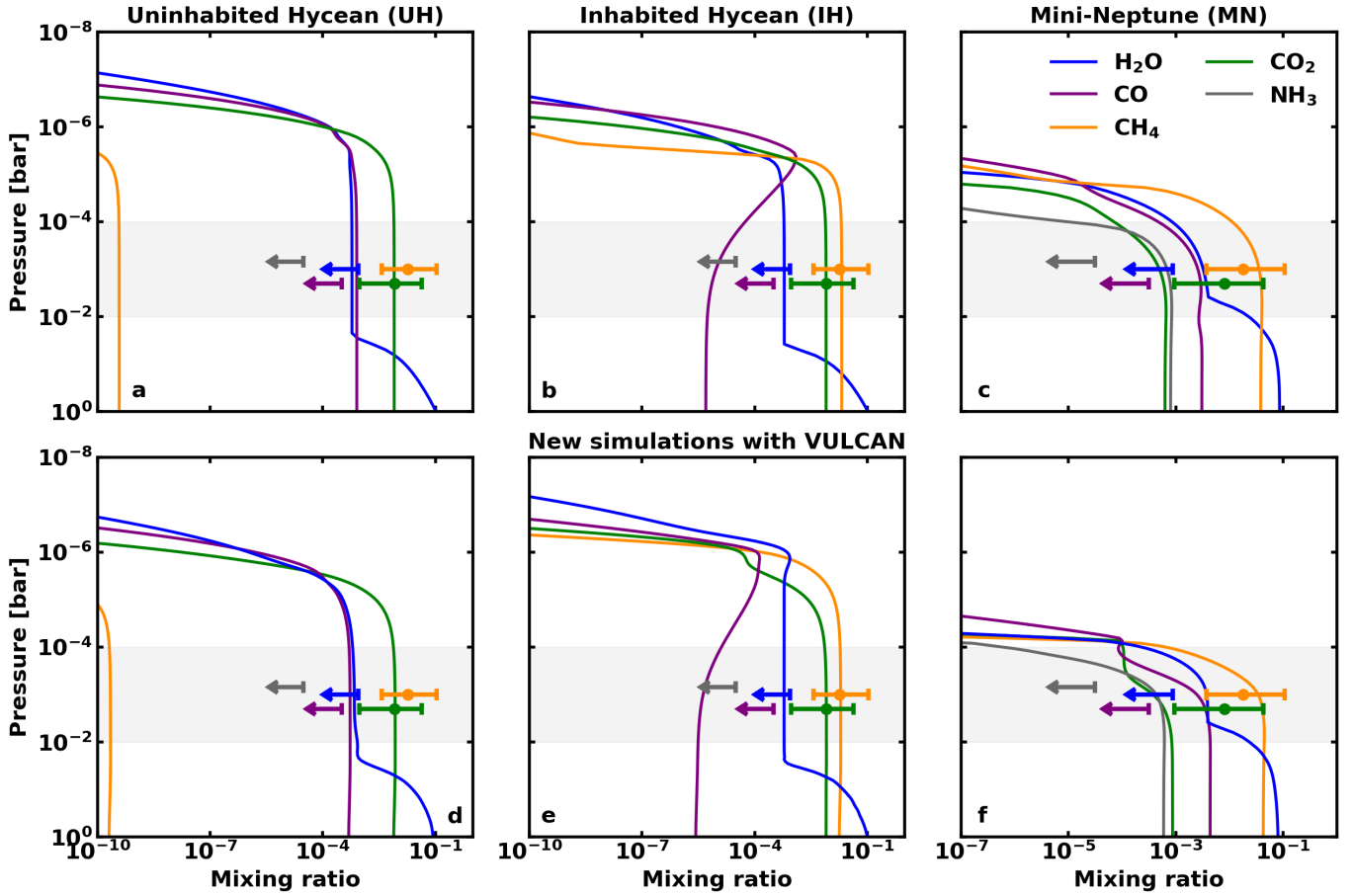


**Figure 1.** Hycean and mini-Neptune scenarios with two photochemical models. Top row: Original simulations from Wogan et al. (2024), showing the mixing ratio of molecules against atmospheric pressure in bar. Bottom row: VULCAN simulations of the same scenarios with equivalent assumptions (see main text). The scenarios are: an uninhabited Hycean (left column), an inhabited Hycean (middle column), and a mini-Neptune case (right column). The given molecular constraints are from the “One offset” case (Madhusudhan et al. 2023b) as this case gives the best fit to the observed data.  $1\text{-}\sigma$  error bars are given for detected molecules ( $\text{CH}_4$  - orange;  $\text{CO}_2$  - green), and  $2\text{-}\sigma$  upper limits are given for CO (purple),  $\text{H}_2\text{O}$  (blue), and  $\text{NH}_3$  (grey), which were not detected by Madhusudhan et al. (2023b). The photosphere, the region in the atmosphere which impacts the transmission spectrum observed, is given in a light grey shade between  $10^{-2} - 10^{-4}$  bar. A variety of simulations were run with both the W24 setup (see Table A1) and VULCAN (see Table A2). All of the simulations shown in this figure use the GJ 176 spectrum. Only the inhabited Hycean scenarios in both models are consistent with the retrieved abundances.

is expected by default. The uninhabited Hycean case was disfavoured by W24 because insufficient  $\text{CH}_4$  was produced photochemically, and the initial  $\text{CH}_4$  abundance was assumed to be negligible, which is unlikely to be the case in a temperate  $\text{H}_2$ -rich atmosphere. On the other hand, in the mini-Neptune case in W24, the initial  $\text{CH}_4$  abundance was set by the assumed  $100\times$  solar metallicity, which naturally results in a high abundance that matches the retrieved value. Finally, W24 did not test higher surface pressures than 1 bar for the Hycean world scenarios, while higher surface pressures are expected to result in a greater  $\text{CH}_4$  abundance (Yu et al. 2021; Madhusudhan et al. 2023a).

### 3.3. Temperature structure and albedo

The predicted abundances in photochemical models are naturally sensitive to the assumed temperature structure in the atmosphere. Fig. 2 shows the different  $P$ - $T$  profiles used for the mini-Neptune and Hycean cases from W24. At pressures between  $3 \times 10^{-3} - 1$  bar, the two profiles significantly diverge. As can be seen in other works, which either move the surface pressure between simulated scenarios or assume a deep atmosphere with no surface (e.g., Tsai et al. 2021a; Yu et al. 2021), the  $P$ - $T$  profiles should be consistent when they are at pressure levels shared between the simulations for a given albedo. This is because the presence of

a surface does not significantly alter the  $P$ - $T$  profile in the upper atmosphere (Tsai et al. 2021a).

The Bond albedo plays a central role in driving both the radiation field in a photochemical model as well as the temperature profile. The observed transmission spectrum of K2-18 b provides evidence for the presence of clouds/hazes in the planet (Madhusudhan et al. 2023b). W24 assume different prescriptions for the incoming radiation between the Hycean and mini-Neptune cases. W24 reduce the incoming radiation by 30% in the Hycean case and not at all in the mini-Neptune case. We also include two additional mini-Neptune temperature profiles in Fig. 2 when assuming that 30% and 40% of radiation is immediately reflected off the top of the atmosphere. A 40% albedo is required to match the temperature profile in the W24 Hycean case at pressures less than 0.4 bar. This albedo of 0.4 is also required for  $\text{H}_2\text{O}$  to just be consistent with the retrieved upper limit for  $\text{H}_2\text{O}$ , with  $\text{CH}_4$  being the only other molecule that matches the molecular constraints.

The 30% of the incoming radiation would not be reflected at the top of the atmosphere in reality but instead reduced through scattering, photoabsorption and photodissociation, when passing through denser atmospheric layers. Moreover, W24 use the GJ 176 spectrum to act as a proxy for K2-18 (following Scheucher et al. 2020; Hu et al. 2021). GJ 436 has been used in other work (Tsai et al. 2024a), and in Appendix C we suggest that GJ 849 could also be used. So, different simula-

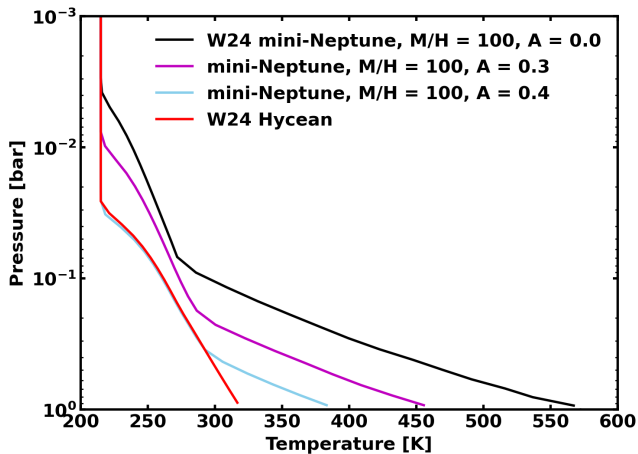


**Figure 2.**  $P$ - $T$  profiles for Hycean and mini-Neptune scenarios. The two pressure-temperature profiles that are used in W24, for the Hycean (red) and mini-Neptune (black) atmospheric simulations at pressures less than 1 bar. At pressures less than  $3 \times 10^{-3}$  bar, the temperature is at 215 K in both models. A second and third mini-Neptune model that we simulated shows the mini-Neptune temperature profile when 30% and 40% of radiation is reflected off the top of the atmosphere, shown in magenta and light blue, respectively.

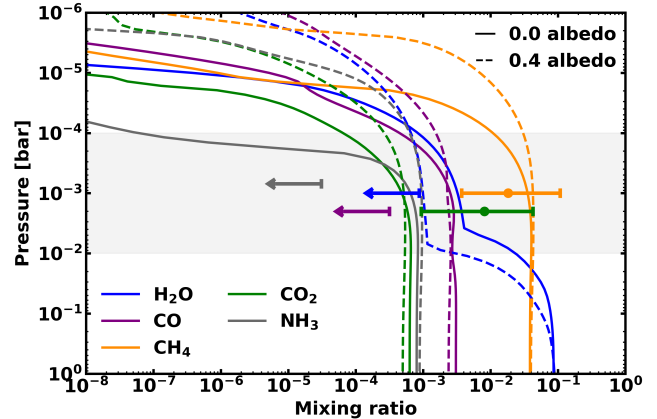


**Figure 3.** Mini-Neptune scenario with different Bond albedos. These simulations used the W24 setup for the mini-Neptune scenario for K2-18 b, showing the standard  $100\times$  solar metallicity scenario with no albedo by the solid lines and the 0.4 top of atmosphere albedo case in the dashed lines. The photosphere is marked in light grey.  $1\text{-}\sigma$  constraints are given for detected molecules ( $\text{CH}_4$  and  $\text{CO}_2$ ) using the one-offset values from Madhusudhan et al. (2023b), whilst  $2\text{-}\sigma$  upper limits are given by the arrows for  $\text{NH}_3$ ,  $\text{H}_2\text{O}$ , and  $\text{CO}$ . In the 0.4 albedo case,  $\text{H}_2\text{O}$  is on the border of the upper limit, with  $\text{CO}_2$  is still lower than its  $1\text{-}\sigma$  limit, and  $\text{CO}$  and  $\text{NH}_3$  remain too high.

tions in the literature use different spectra and alter the incoming radiation through different methods. All these factors influence the propagation of ultraviolet (UV) radiation and affect the resulting atmospheric chemical composition differently between the Hycean and mini-Neptune cases.

### 3.4. Synthetic spectra

W24 stated that both a mini-Neptune case and an inhabited Hycean case can explain the observations from Madhusudhan et al. (2023b). To reach this conclusion, they generated transmission spectra of forward models from the photochemical results and calculated a reduced  $\chi^2$  ( $\chi_r^2$ ) for each scenario. The  $\chi_r^2$  test assumed that the number of degrees of freedom was the number of data points (i.e. no free parameters). For the uninhabited Hycean, the inhabited Hycean, and the mini-Neptune clear-sky scenarios, a  $\chi_r^2$  of 3.22, 1.51, and 1.51, respectively, was found. When aerosols were included in the scenarios, the  $\chi_r^2$  for each scenario was 2.30, 1.40, and 1.46, respectively. Then, after removing the JWST data shortward of  $1 \mu\text{m}$ , the  $\chi_r^2$  was 2.10, 1.15 and 1.15, respectively.

This approach is reminiscent of the pre-retrieval era whereby individual forward models were fit to low-resolution exoplanet spectra which precluded a robust assessment of model degeneracies and confidence esti-

mates (Madhusudhan & Seager 2009). For example, it is unclear how many other photochemical models would match at that  $\chi_r^2$  reported by W24 or at a better  $\chi_r^2$ , such that there is no evaluation of whether the forward models are unique solutions. Furthermore, not accounting for the various free parameters in each model scenario biases the model comparisons. The  $\chi_r^2$  as presented by W24 could be seen as a measure of the goodness-of-fit of the specific parameter choices within each model scenario. However, it does not serve as evidence to assess whether one model scenario explains the data better than another. For example, a different instance in the uninhabited Hycean model space may provide a better  $\chi_r^2$  than reported, but even then it would not provide sufficient grounds for comparison between that model scenario and another. A reliable approach to evaluate model scenarios is to compare either (a) the best-fit  $\chi_r^2$  over the full parameter space of each model scenario, accounting for the true number of degrees of freedom, or (b) more accurately, the Bayesian evidence by integrating the prior-weighted likelihood over the model parameter space, as computed in extant atmospheric retrievals (e.g., Madhusudhan et al. 2023b).

The procedure does also not reveal why the different synthetic spectra achieved the same  $\chi_r^2$ , despite having significantly different abundances of molecules in their simulated atmospheres. It is also possible to fit an  $n^{\text{th}}$  degree polynomial to the data which achieves a similar  $\chi_r^2$ , but this reveals nothing about the atmospheric molecular abundances because such a fit is not based on a physically plausible model, unlike atmospheric retrievals. This is why atmospheric retrievals are implemented to provide confidence estimates on specific variables based on a free parameter space exploration of millions of individual models. Therefore, photochemical model results should instead be compared to the retrieved abundances, especially in the JWST era where high-quality spectra allow for detailed Bayesian inferences.

### 3.5. Occam’s Razor for Model Preference

The primary conclusions of W24 are that (a) an uninhabited Hycean scenario in K2-18 b is inconsistent with the observations, (b) the inhabited Hycean and mini-Neptune scenarios are in comparable agreement with observations, and (c) the mini-Neptune scenario is preferred over the inhabited Hycean through an Occam’s Razor argument that the mini-Neptune model is simpler. However, based on the above discussion, the mini-Neptune scenario is in least agreement with the retrieved abundances, while the Hycean scenarios perform better, rendering Occam’s Razor inapplicable in the present

context. Nonetheless, we evaluate the arguments of W24 in favour of the mini-Neptune scenario and against the Hycean scenario.

W24 state that a mini-Neptune with a 60 K intrinsic temperature, and an atmosphere that has  $100\times$  solar metallicity and a solar C/O ratio, can broadly explain the observed  $\text{CH}_4$  and  $\text{CO}_2$  abundances. However, their calculated  $\text{CO}_2$  actually lies at a lower abundance than the  $1\text{-}\sigma$  retrieved limit. An intrinsic temperature of 60 K was chosen based on the modelling from Hu (2021), who stated that this value is similar to the internal temperature of Neptune. The internal heat of Neptune was estimated to be  $0.433 \pm 0.046 \text{ W m}^{-2}$  (Pearl & Conrath 1991), which corresponds to an internal temperature of 52.57 K. This internal temperature estimate was derived from Voyager observations of Neptune, which may need to be updated in light of the Cassini results for Jupiter (Li et al. 2018). Additionally, the intrinsic temperature of a mini-Neptune is unknown and the internal temperature of K2-18 b could be lower than 60 K (Valencia et al. 2013; Madhusudhan et al. 2020): internal temperature generally scales with planet mass (Mordasini et al. 2012; Lopez & Fortney 2014); Neptune is roughly twice the mass of K2-18 b; and GJ 1214 b, which has a comparable mass to K2-18 b (within 10%), has been suggested to have an internal temperature of 30 K (Valencia et al. 2013). Given a colder internal temperature, then  $\text{CO}_2$  would be even less abundant<sup>7</sup>.

W24 claim that the simulated deep-atmosphere kinetics produces abundances of CO and  $\text{NH}_3$  which are generally compatible with their non-detection. In fact, at 1 mbar,  $\text{NH}_3$  and CO are both calculated to be at greater abundances (by a factor of 23, and 8 respectively) than their retrieved  $2\text{-}\sigma$  upper limits.

The absence of  $\text{H}_2\text{O}$  features in the transmission spectrum are attributed to water vapor condensation and cold trapping by W24. We agree with this statement, but this is not what the simulated mini-Neptune scenario from W24 shows: the predicted  $\text{H}_2\text{O}$  mixing ratio is a factor of 4 too high at 1 mbar, and a factor of 28 too high at 10 mbar, compared to the  $2\text{-}\sigma$  upper limit on  $\text{H}_2\text{O}$ . In the mini-Neptune scenario using the W24 setup, to get enough condensation to explain the non-detection of  $\text{H}_2\text{O}$ , we find that a top of atmosphere albedo of  $\geq 0.4$  is required by the W24 setup, although

<sup>7</sup> We tested the effect of internal temperature with the standard 100 times solar metallicity model from W24. For internal temperatures of 52.6 K, 50 K, 40 K, and 30 K, the  $\text{CO}_2$  mixing ratio at 1 mbar was  $3 \times 10^{-4}$ ,  $2 \times 10^{-4}$ ,  $5 \times 10^{-5}$ , and  $2 \times 10^{-5}$ , respectively. The  $1\text{-}\sigma$  lower limit on  $\text{CO}_2$  in the ‘one offset’ case is  $9 \times 10^{-4}$



CO and NH<sub>3</sub> remain too high and CO<sub>2</sub> remains too low in abundance (see Fig. 3).

W24 also claim that 1D radiative-convective-equilibrium modeling can explain the climate of K2-18 b in the case of the mini-Neptune. This is despite no observational constraints on the temperature structure of the dayside atmosphere or on radiative-convective equilibrium for K2-18 b. As a climate argument against the Hycean scenario, it has been discussed that a Hycean exoplanet could undergo a steam runaway greenhouse (Scheucher et al. 2020; Innes et al. 2023; Pierrehumbert 2023) unless the Bond albedo is sufficiently high in order to reflect enough incoming radiation (Piette & Madhusudhan 2020; Madhusudhan et al. 2021). For K2-18 b to be a Hycean world, most recent dayside 3D simulations require a Bond albedo of  $\sim 0.5 - 0.6$  (Leconte et al. 2024). Such an albedo cannot be ruled out given the inference of clouds/hazes in K2-18 b (Madhusudhan et al. 2023b), and several planets, including Jupiter, have Bond albedos reported between  $\sim 0.5 - 0.7$  (Li et al. 2018; Crossfield et al. 2020; Kempton et al. 2023; Hoyer et al. 2023).

While a sufficiently high Bond albedo to maintain an ocean on K2-18 b is not implausible, a robust albedo estimate is currently not available. Leconte et al. (2024) (L24) use model spectra to assess the dayside albedo of K2-18 b based on the two weakest CH<sub>4</sub> features in the transmission spectrum (at 1  $\mu\text{m}$  and 1.2  $\mu\text{m}$ ). The observed amplitude of one such feature is used to infer its haze properties at the day-night terminator and then extrapolate the findings to the dayside albedo. At the outset, it is unclear if any of the L24 models are compatible with the observed transmission spectrum, as no such comparison is presented. Secondly, heuristic metrics based on such limited weak spectral features and nominal model considerations (e.g. homogeneous Rayleigh-like hazes) are unlikely to obtain robust constraints on clouds/hazes and resolve various model degeneracies, e.g. between clouds/hazes, molecular contributions and temperature. This is better pursued with atmospheric retrievals with the full data available (1-5  $\mu\text{m}$ ), which indeed show evidence for clouds/hazes as discussed above. It is also important to recognize that the scattering on the dayside can be very different to that at the terminator, rendering extrapolations to dayside albedo indicative at best. Finally, inferences of clouds/hazes and Bond albedos have to be conducted within a self-consistent framework that also considers all available chemical abundance constraints. The models of K2-18 b reported by L24 predict NH<sub>3</sub> and CO abundances 1-2 orders of magnitude higher than the retrieved 2- $\sigma$  upper limits. Future observations and self-consistent

cloud/haze modeling would be helpful to obtain better insights into the possible dayside Bond albedo of K2-18 b.

Finally, W24 argue that XUV-driven hydrogen escape may erode a thin  $\sim 1$  bar H<sub>2</sub>-dominated atmosphere that cannot be replaced by volcanism (Noack et al. 2016; Kite & Ford 2018; Hu et al. 2023). This is indeed a possibility, however, there is no quantitative analysis that supports such a conclusion for K2-18 b specifically, considering a wide range of initial and steady state conditions that may be possible on K2-18 b. It is feasible that the primordial atmosphere may have been significantly deeper than the present state. Furthermore, given an adequate albedo, K2-18 b could have a deeper atmosphere (e.g., 10 bar) and still maintain Hycean conditions (Piette & Madhusudhan 2020; Madhusudhan et al. 2023a). For CH<sub>4</sub> to be present in the observed abundance, W24 argue that K2-18 b as a Hycean world requires a biogenic, or other, source of CH<sub>4</sub>. This assumes that the surface pressure of the Hycean world scenario is 1 bar, which is just one possibility given all the current unknown physical parameters regarding K2-18 b.

Overall, we find the conclusions of W24 to be inconsistent with the retrieved abundances and dependent on initial conditions between the different model scenarios. Nevertheless, it is important to further investigate the viability of the Hycean vs mini-Neptune scenarios. We therefore revisit the two Hycean scenarios (inhabited and uninhabited) and the mini-Neptune scenario for K2-18 b through further photochemical modeling with two independent photochemical models and expand the simulated parameter space to determine which scenarios can best explain all the retrieved abundance constraints.

#### 4. RESULTS

In this section, we reexamine the mini-Neptune scenario and the two Hycean scenarios for K2-18 b using both the W24 photochemical modeling setup and the VULCAN photochemical model. We explore a range of initial conditions for the mini-Neptune scenario to cover a broader parameter space, aiming to identify any simulated cases that can explain the observed abundance constraints. Additionally, we investigate various parameters, such as photochemical cross sections and the stellar input spectrum, to assess the sensitivity in calculated atmospheric composition using the W24 setup for all three scenarios. Finally, we increase the surface pressure and test the results for the uninhabited Hycean scenario.

##### 4.1. Sensitivity to Cross Sections and Stellar spectra

For both mini-Neptune and Hycean scenarios with the W24 setup, we explore different input data and initial

conditions to determine the effects on the calculated mixing ratio profiles for various molecules of observational and biological interest. We find significant differences in the photochemical cross sections between three publicly available photochemical models: *Atmos*, *Photochem*, and *VULCAN*, as shown in Appendix B.

We recompute the W24 scenarios using the same model setup but replacing the photochemical cross sections with those from different sources. In this section, we present the results from these cross section comparisons. We found that there were discrepancies for twenty-two molecules which we swapped into the W24 setup. Because the wavelength binning of the cross sections are sometimes different between sources and molecules, we vary the wavelength binning of the cross sections, keeping the original resolution (native) as well as binning to the resolution of the cross sections for *Photochem* molecules (binned). Furthermore, we test the impact of three different stellar spectra: GJ 176, GJ 436, and GJ 849, which have different strengths and shapes of incoming UV radiation (see Appendix C for a discussion on stellar proxies and Fig. C1 and Fig. C2).

#### 4.1.1. *Mini-Neptune scenario*

The W24 mini-Neptune case only matched one out of the five abundance constraints, so we performed many more simulations over a larger parameter space to check if other simulations are more consistent with the current observations and atmospheric retrieval analysis.

Using the *Photochem* and *PICASO* combination as in W24, we tested different initial conditions on a grid of C/O ratio from 0.5 to 2.0 and metallicity of 30 to 200, a  $T_{\text{int}}$  of 30 K to 70 K, and with three different stellar spectra. None of the predicted abundances from any of these cases could match the constraints for all five molecules. Fig. 4 shows a range of results assuming different initial metallicities with the W24 setup (30 $\times$ , 50 $\times$ , 100 $\times$ , and 200 $\times$  solar metallicity), whereby the cross sections have been altered whilst using either the GJ 176, GJ 849, or GJ 436 spectrum.

We find that the cross section source, the resolution of the cross sections used, and the assumed stellar spectra, all alter the predicted composition, as shown in Fig. 4. When keeping the star constant, and changing the cross sections, peak abundance changes (between 10 and 0.1 mbar in pressure) can be up to a factor of  $\sim 3 \times 10^9$ . When keeping the cross sections constant but varying between the three stellar input spectra used, peak abundance changes can be up to a factor of  $\sim 1 \times 10^9$ . The maximum differences in calculated abundances in the photosphere at the same pressure level are  $3 \times 10^9$  ( $\text{NH}_3$ ),  $2 \times 10^9$  ( $\text{NH}_3$ ),  $1 \times 10^9$  ( $\text{H}_2\text{S}$ ), and  $4 \times 10^7$  ( $\text{H}_2\text{S}$ ), in the

200, 100, 50, and 30 times solar metallicity cases, respectively.

Peak abundances change for  $\text{SO}_2$  by up to a factor of  $\sim 10^7$  when using different stellar spectra and cross sections. Other mixing ratio changes occur for  $\text{H}_2\text{O}$ ,  $\text{CH}_4$ ,  $\text{CO}_2$ , and  $\text{CO}$ , although these are smaller in magnitude because the W24 setup fixes their relatively high abundance at the 1 bar lower boundary in the photochemical simulation due to mixing in the deeper atmospheric simulation. The production rate effectively adjusts to compensate for any chemical loss alterations induced by the change in cross section data.

At a greater metallicity than 100 times solar,  $\text{CH}_4$ ,  $\text{CO}_2$  and  $\text{CO}$  increase at the lower boundary (1 bar) in the photochemical simulations, and the inverse occurs at lower metallicities. When changing the C/O ratio to lower values, carbon bearing species such as  $\text{CH}_4$ ,  $\text{CO}_2$  and  $\text{CO}$  decrease at the lower boundary, but  $\text{H}_2\text{O}$  increases, and vice versa when increasing the C/O ratio.

There are several trends with metallicity and the assumed cross sections used. With increasing metallicity, a change in cross section from the original *Photochem* cross sections has a larger perturbation effect for the mixing ratios of  $\text{CO}_2$ ,  $\text{CO}$ ,  $\text{CH}_4$ ,  $\text{HCN}$ , and  $\text{H}_2\text{O}$ . On the other hand,  $\text{H}$ ,  $\text{NH}_3$ , and  $\text{H}_2\text{S}$  have larger mixing ratio perturbations with decreasing metallicity. For these cross section changes,  $\text{SO}_2$  is an example where the abundance can be increased or decreased depending on the choice of cross sections and what resolution is used.

The 200 $\times$  solar metallicity simulations produce results which become more consistent with the retrieved JWST abundance of  $\text{CO}_2$ . This can, however, depend on the source of the cross sections as the *Atmos* native cross sections significantly decrease  $\text{CO}_2$  abundance in the photosphere away from the other profiles, and could mean the difference between remaining consistent or inconsistent with retrieved abundances. Ultimately, whilst certain changes can produce chemical abundances that more closely match the retrieved abundance constraints from [Madhusudhan et al. \(2023b\)](#), none of the mini-Neptune simulations we performed can explain the simultaneous non-detection of  $\text{H}_2\text{O}$ ,  $\text{CO}$ , and  $\text{NH}_3$ , and the presence of  $\text{CO}_2$  and  $\text{CH}_4$  in mixing ratios of  $\sim 1\%$ .

Overall, we find that various initial conditions and alternative sets of input data can introduce significant uncertainties on the final predicted atmospheric composition. Such results from different models can then lead to different conclusions and future modeling efforts should be aware of these sensitivities. In the specific mini-Neptune scenario for K2-18 b as simulated here, the

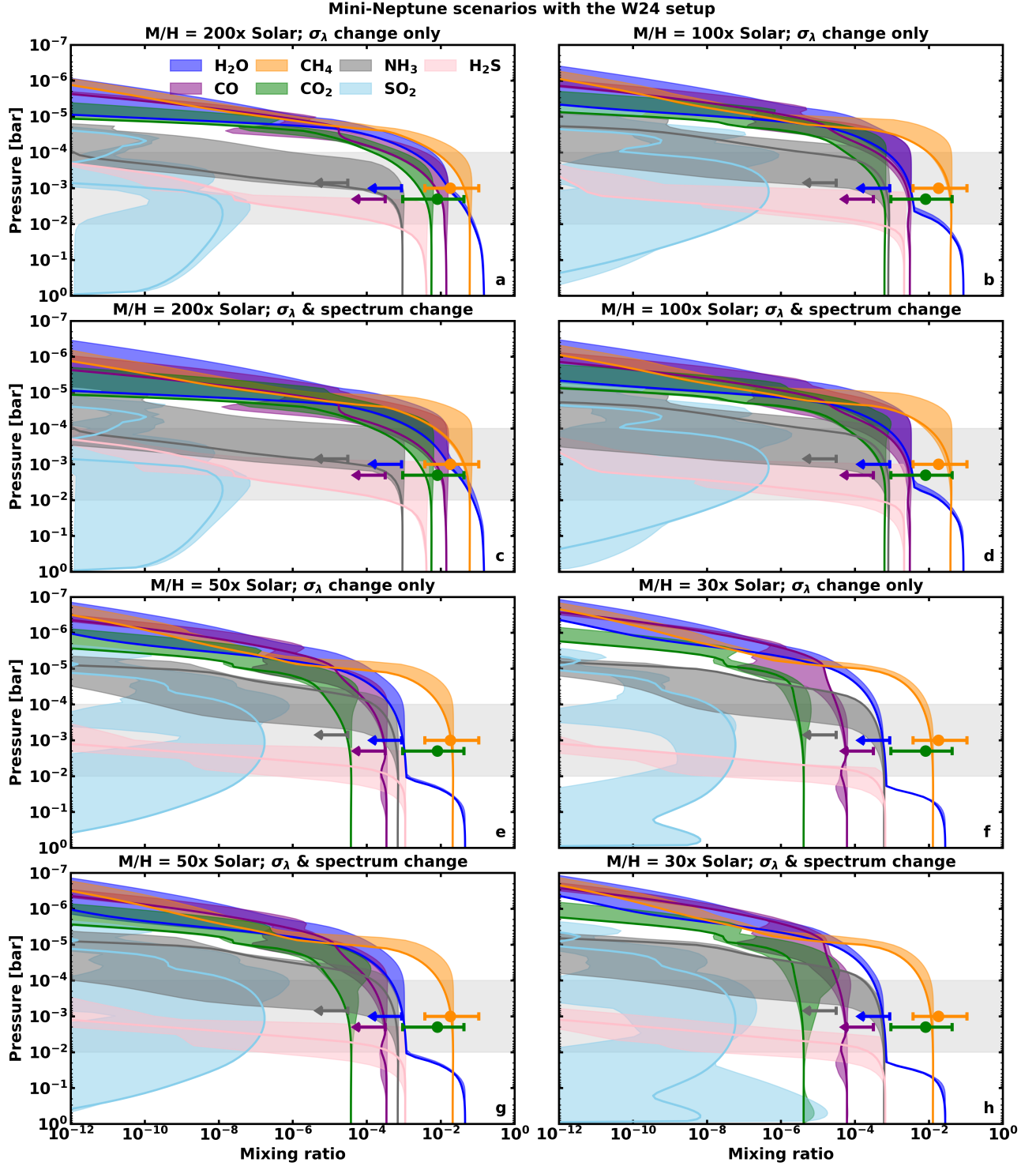


**Figure 4.** Mini-Neptune scenario for K2-18 b using the W24 setup (PICASO and Photochem). The predicted mixing ratios for different metallicities ( $200\times$ ,  $100\times$ ,  $50\times$ ,  $30\times$  solar metallicity, denoted by  $M/H$ ) are shown by the shaded regions, indicating the maximum deviations between the different simulations. The various simulations used different cross section sources and resolutions in the first and third row, assuming the host star is represented by GJ 176, and the internal temperature ( $T_{\text{int}}$ ) is 60 K. The second and fourth row show the same, but this time including all the same simulations but with GJ 176, GJ 849, and GJ 436 as the host stars. The photosphere is marked in light grey.  $1\text{-}\sigma$  constraints are given for detected molecules (CH<sub>4</sub> and CO<sub>2</sub>) using the values from Madhusudhan et al. (2023b), whilst  $2\text{-}\sigma$  upper limits are given by the arrows for NH<sub>3</sub>, H<sub>2</sub>O, and CO. The colours used for the constraints are the same as those used in Fig. 3, with SO<sub>2</sub> and H<sub>2</sub>S also shown in light blue and pink, respectively. The thick lines in each panel show the results when GJ 176 is used with Photochem cross sections.

sensitivity tests still do not support the mini-Neptune scenario when comparing to retrieved abundances.

#### 4.1.2. Hycean scenarios

We now examine the effect of different cross section sources and stellar spectra on the Hycean cases when using the W24 setup. Fig. 5 shows the uninhabited (left column) and inhabited (right column) Hycean cases with binned and native *Atmos* and *VULCAN* cross sections using three different stellar spectra (See Table A1 for a description of simulations performed with the W24 setup).

In the uninhabited Hycean case with the binned and native *Atmos* cross sections, CO increases at the surface by a factor of 25 and 2 to a mixing ratio of 0.02 and 0.0015, respectively. Yet for the *VULCAN* cross sections, CO decreases by a factor of 1.5 and 1.9 when binned or used at their native resolution, respectively. In the inhabited Hycean cases, CO decreases by a factor of between 2.1 – 3.1, depending on the various cross section choices. The CH<sub>4</sub> mixing ratio increases by 360 and 225 for the binned and native *Atmos* cross sections, and 1150 and 350 times for the binned and native *VULCAN* cross sections, respectively.

Generally speaking the W24 inhabited Hycean case appears much less sensitive to the changes in cross sections and stellar spectra when compared to the uninhabited case. This may be because CH<sub>4</sub> photodissociates at UV wavelengths; these photons would otherwise be able to penetrate further into the atmosphere and affect other molecules. When swapping the cross sections in the inhabited hycean scenario, between 1 bar and 10<sup>-5</sup> bar, CH<sub>4</sub> increases by a factor of 1.11 – 1.25, whereas CO decreases by 2.2 – 3.1 times. H<sub>2</sub>O is essentially unaffected at the surface due to the assumed tropospheric humidity. In the upper atmosphere, H<sub>2</sub>O is significantly perturbed with the binned *Atmos* cross sections, decreasing by a factor of  $\approx 100$  by 10<sup>-6</sup> bar.

Altogether, we find peak abundances can change in the uninhabited Hycean case for up to  $\sim 10^3$  for CH<sub>4</sub> and  $\sim 10^2$  for CO. In the inhabited Hycean case, CO and CH<sub>4</sub> are less affected, altering their abundance by up to a factor of 3. This demonstrates that both the assumed resolution of the cross sections, and the sources the cross sections are from, have a significant impact on the final abundance of specific molecules. The composition of the atmosphere and boundary conditions drive the large difference in predicted discrepancies between the two Hycean scenarios.

Taken in their totality, modeling choices can therefore introduce large uncertainties on the final predicted atmospheric composition if a parameter space is not ad-

equately explored. If we take CH<sub>4</sub> in the uninhabited Hycean case as an example, by only changing the spectrum to GJ 849, one can increase the predicted CH<sub>4</sub> mixing ratio by a factor of 2.1. However, when introducing both a different spectrum (GJ 849) and cross section source (*VULCAN*), one can increase the CH<sub>4</sub> mixing ratio by a factor of 1260. A modeller will not necessarily know beforehand what the effect of such modifications will be, especially when we have shown that the opposite effect for a specific molecule can occur between the inhabited and uninhabited Hycean scenarios.

#### 4.2. Revisiting K2-18 b scenarios with *VULCAN*

Now we present the atmospheric scenarios using the *VULCAN* photochemical model, presenting first the mini-Neptune scenario and then the Hycean scenarios, before varying the atmospheric pressure and temperature profile of the uninhabited Hycean scenario in *VULCAN*.

##### 4.2.1. Mini-Neptune scenario

We set up *VULCAN* with the W24 *P-T* and  $K_{zz}$  (vertical mixing parameter) profiles and different initial elemental abundances (metallicities), assuming the same properties for K2-18 b. We show examples of 50 $\times$ , 100 $\times$ , and 200 $\times$  solar metallicity *VULCAN* mini-Neptune simulations in Fig. 6. The results are similar in abundance to the W24 results: if CH<sub>4</sub> and CO<sub>2</sub> match the constraints, then there are other species which do not match, including H<sub>2</sub>O and CO which have mixing ratios that are greater than the 2- $\sigma$  upper limits. As an illustrative example, CH<sub>4</sub> and CO<sub>2</sub> are consistent with the retrieved abundances in the 200 $\times$  solar metallicity scenario, but the non-detected molecules are all predicted to be significantly greater than their 2- $\sigma$  upper limits. Additionally, for 50 $\times$ , 100 $\times$ , and 200 $\times$  solar metallicity, at 1 mbar, NH<sub>3</sub> is a factor of 8, 14, and 27 higher, respectively, than the NH<sub>3</sub> 2- $\sigma$  upper limit.

This result, that photochemical modeling of mini-Neptunes is incompatible with the retrieved JWST constraints, is also consistent with predicted abundances in Yang & Hu (2024a) and Huang et al. (2024).

Yang & Hu (2024a) simulated K2-18 b as a mini-Neptune using the EPACRIS model, exploring a parameter space in *P-T* profiles,  $K_{zz}$ , and chemical composition. Their model was able to get compatible CH<sub>4</sub> and CO<sub>2</sub> abundances in their 100  $\times$   $Z_0$  and 10  $\times$   $Z_0$  cases with the retrieved “two offset” constraints from Madhusudhan et al. (2023b), and their 10  $\times$   $Z_0$  case was also consistent with CO. However, NH<sub>3</sub> and H<sub>2</sub>O were more than an order of magnitude too high. Furthermore, considering the best fit “one offset” constraints from Mad-

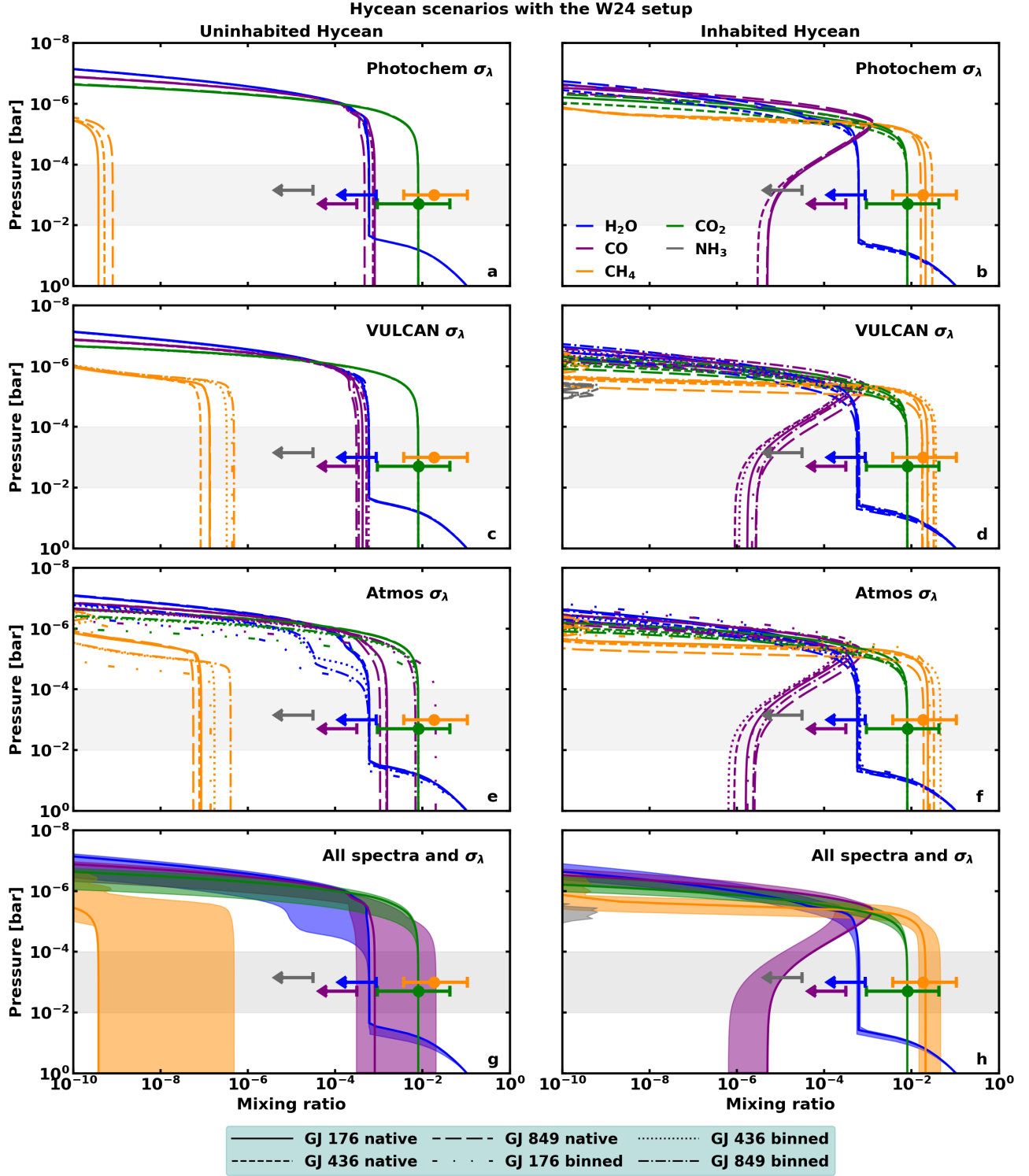


**Figure 5.** Hycean scenarios for K2-18 b using the W24 setup. The photochemical modelling uses Photochem in the W24 setup for an uninhabited Hycean case (left column) and an inhabited Hycean case (right column). The first, second, and third rows use Photochem, VULCAN, and Atmos cross sections, respectively (see Appendix B). The solid lines, dashed lines and long-dashed lines are with native cross sections using the GJ 176, GJ 436, and the GJ 849 spectra, respectively. The dash-dot-dot-dashed lines, dotted lines, and dash-dotted lines are with binned cross sections using the GJ 176, GJ 436, and the GJ 849 spectra, respectively. The final row shows shaded regions which display the range of results between all perturbations in the top 3 rows. The thick lines in the final row also shows the original W24 results. The “observable” portion of the atmosphere and the molecular constraints are marked as in Fig. 1.

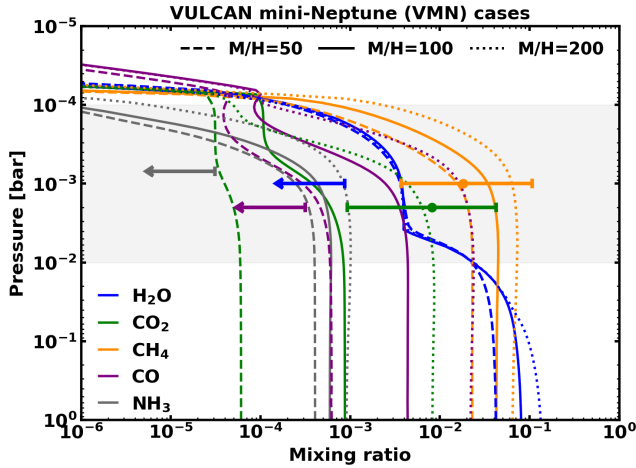


**Figure 6.** Mini-Neptune scenario for K2-18 b using VULCAN. The mini-Neptune simulations use the same  $P$ - $T$  and  $K_{zz}$  profiles that were used in W24 from  $10^{-8}$  – 500 bar. The colours and constraints are the same as in Fig. 1. The solid line is a  $100\times$  solar metallicity case, the dashed line is a  $50\times$  solar metallicity case, and the dotted line is a  $200\times$  solar metallicity case. None of the cases are consistent with all five retrieved abundances. The predicted abundances are comparable to those produced in using the W24 setup.

Madhusudhan et al. (2023b), CO is too high in their  $10\times Z_0$  case.

Huang et al. (2024) simulated K2-18 b with and without water condensation, with albedos varying between 0 and 0.75, and surface pressures of 1 and 1000 bar. They concluded that the JWST observations were best explained by a deep mini-Neptune atmosphere with a 0.56 albedo with  $\text{CH}_4$  feature amplitudes greater than 100 ppm (note that this contradicts the results from Leconte et al. 2024). However, in this case, the predicted mixing ratios in the photosphere are  $\approx 50$  and  $\approx 2.5$  times higher than the  $2\text{-}\sigma$  upper limits on  $\text{NH}_3$  and CO, respectively, and 3 times lower than the  $1\text{-}\sigma$  limit for  $\text{CO}_2$ . The choice of 70 K for the internal temperature may be too high (see section 3). Note that the corresponding shallow 1 bar case for K2-18 b in Huang et al. (2024) does not explain the data either:  $\text{H}_2\text{O}$ , CO, and  $\text{NH}_3$  are below the  $2\text{-}\sigma$  upper limits, but  $\text{CH}_4$  and  $\text{CO}_2$  are several orders of magnitude under-abundant. Whilst Huang et al. (2024) account for the albedo in setting the  $P$ - $T$  profile, they do not modify the total incoming UV flux whilst using an active M2V star at 45 Myr age, which may both result in an overestimation of the photolysis rates. This is important as it is photodissociation that leads to  $\text{CH}_4$  destruction in models of shallow Hycean atmospheres.

In order for the mini-Neptune scenario to explain the observed abundances for K2-18 b, it may require the fol-

lowing: a large enough Bond albedo (e.g.,  $\geq 0.4$ ) such that water sufficiently condenses below the photosphere; some mechanisms that can deplete both  $\text{NH}_3$  and CO, which may require a low C/O ratio of  $\sim 0.02$  (Madhusudhan et al. 2023b); and have a higher internal heat flux than would otherwise be expected for its mass and age to produce enough  $\text{CO}_2$ .

#### 4.2.2. Uninhabited Hycean scenario

In W24, the Photochem uninhabited Hycean simulation starts with negligible  $\text{CH}_4$ , which then accumulates through photodissociation of  $\text{CO}_2$  and subsequent reactions. The  $\text{CH}_4$  abundance remains significantly lower than the observed abundance. We find that this result is the same even when the model starts with a high  $\text{CH}_4$  abundance by volume (e.g. 5%). This result was used by W24 to argue that the uninhabited Hycean case scenario is incompatible with the observational data.

However, previous work has shown that  $\text{CH}_4$  can be retained at higher abundances when the surface pressure is greater due to thermochemical recycling (Yu et al. 2021; Madhusudhan et al. 2023a). Madhusudhan et al. (2023a) found that  $\text{CH}_4$  abundance was significantly depleted in a 1 bar versus a 100 bar Hycean case (e.g. volume mixing ratio of  $\sim 10^{-5}$  versus  $\sim 10^{-2}$ ). Motivated by this, we explore surface pressures between 1 and 100 bar. We also investigate the effect of the UV albedo of the planet on the  $\text{CH}_4$  abundance. We note that the UV albedo here does not correspond to the Bond albedo, but rather the scaling factor for the incoming stellar UV spectrum used, which was of GJ 436 in this instance. The motivation for this is the fact that Neptune itself is reported to have an albedo of up to 0.85 for UV and blue wavelengths of 300-500 nm (Irwin et al. 2019, 2022, 2023), but a total planetary Bond albedo of 0.3 (Pearl & Conrath 1991). We explore a range of UV albedos up to Neptune’s value of 0.85 which reduces the photodissociation rates in the model. We use the PT3  $P$ - $T$  profile from Madhusudhan et al. (2023a). The choice of PT3 is due to it having the most similar stratospheric temperature to the  $P$  –  $T$  profiles used in W24 but extending to deeper pressures.

We show the results for a 25 bar and 50 bar surface pressure in Fig. 7a and Fig. 7b, respectively. The combination of the higher surface pressure and larger UV albedo results in a longer atmospheric lifetime for  $\text{CH}_4$ . We find that a case with a 50 bar surface pressure, with an initial metallicity of 100 times solar (starting with  $\sim 5\%$   $\text{CH}_4$  by volume), and a 0.75 UV albedo, can explain the abundances in the case of an uninhabited Hycean if sulfur is not included in the chemical network (sulfur species may be deposited into the ocean on a

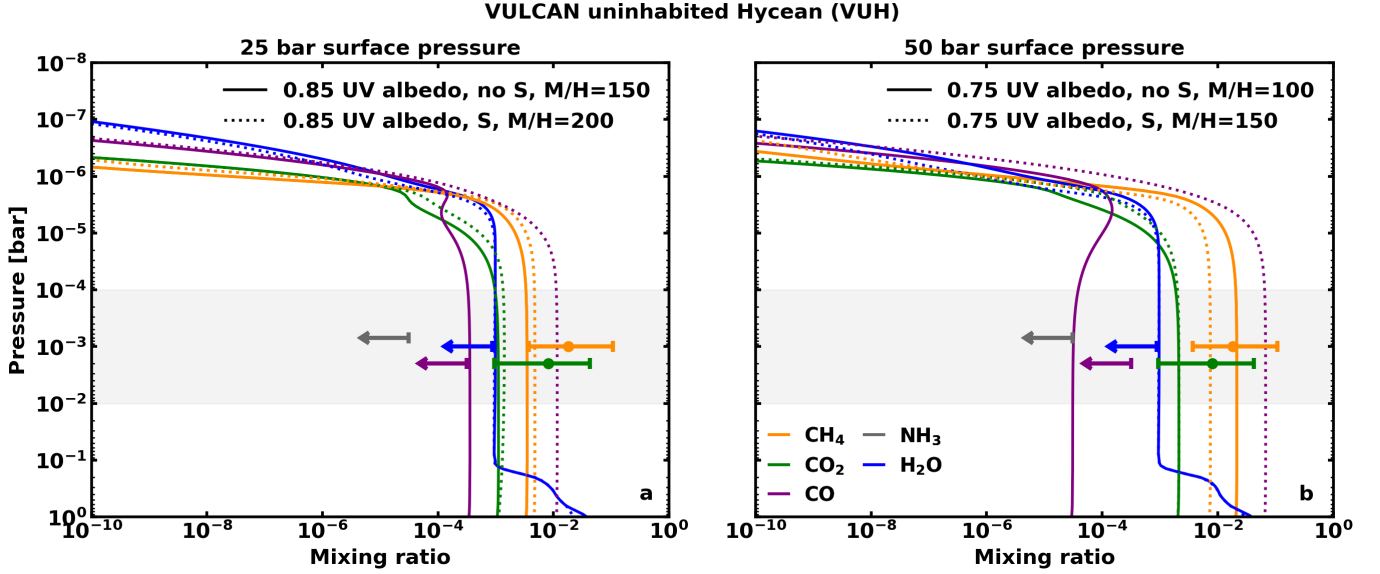


**Figure 7.** Uninhabited Hycean scenario for K2-18 b using VULCAN. Photochemical modeling of an uninhabited Hycean scenario with a 25 bar surface (a; left) and with a 50 bar surface (b; right). The GJ 436 spectrum with a varied UV albedo is implemented in the model. The  $P$ - $T$  profile is PT3 from Madhusudhan et al. (2023a). Different initial metallicities are used between 100 – 200 times solar metallicity. In the uninhabited Hycean scenario, the inclusion of sulfur (labelled S in the legend) in the photochemical network affects the abundance of CO. The uninhabited simulations have no imposed flux for  $\text{CH}_4$  at the planetary surface.  $\text{CO}_2$  has a fixed mixing ratio condition of  $1 \times 10^{-3}$  (25 bar cases) and  $2 \times 10^{-3}$  (50 bar cases). The mixing ratio of  $\text{CH}_4$ ,  $\text{CO}_2$ , CO,  $\text{H}_2\text{O}$ , and  $\text{NH}_3$  are plotted against atmospheric pressure. The constraints and colours are the same as in Fig. 1. Depending on the assumed physical conditions and the chemical network used, the uninhabited Hycean scenario can be shown to be consistent with the retrieved abundance constraints from JWST observations (Madhusudhan et al. 2023b) for all five molecules.

Hycean world; Hu et al. 2021; Loftus et al. 2019; Tsai et al. 2024a). When sulfur is included,  $\text{CH}_4$  is depleted but is still consistent with observations, but now the CO volume mixing ratio is significantly higher than the upper limit. With a 25 bar surface pressure, the predicted abundances provide a good fit for all five JWST constraints when initialising the model with 150 times solar metallicity and invoking a UV albedo of 0.85. Again, CO is overabundant when including sulfur. In that scenario, OH and H, which react with CO, are several orders of magnitude lower in abundance. Other species like S and  $\text{H}_2\text{S}$  can destroy CO and are only present when including sulfur.

The  $\text{CH}_4$  is continuing to deplete after  $10^{17}$  s. This indicates that the lifetime of  $\text{CH}_4$  is on the order of or longer than  $10^{17}$  s, which is more than the estimated age of K2-18 b (Guinan & Engle 2019). As found previously, if there are uninhabited Hycean worlds which form with a large  $\text{CH}_4$  abundance (high metallicity), then older uninhabited Hyceans may exhibit depleted  $\text{CH}_4$ , whilst younger uninhabited Hyceans may have retained enough  $\text{CH}_4$  to be observable with JWST (Madhusudhan et al. 2023a).

We tested other albedos, pressures, and metallicities. In several cases,  $\text{CH}_4$  matches the retrieved abundance

but CO is too high. However, CO can dissolve in an ocean (Van Trump & Miller 1973), and a model of a prebiotic Archean Earth derived a CO deposition velocity of  $10^{-8}$   $\text{cm s}^{-1}$  (Kharecha et al. 2005). This deposition velocity depends on the partial pressure of CO, the overturning velocity of the ocean, the pH of the ocean, and the depth of the ocean, amongst other parameters (Kharecha et al. 2005). Such estimates are beyond the scope of this work because such an ocean on K2-18 b may span a wide parameter space (Rigby & Madhusudhan 2024). Future work should investigate this in more detail, but it could be a viable mechanism whereby CO is adequately depleted.

In all simulations, due to the assumed presence of an ocean in which  $\text{NH}_3$  dissolves,  $\text{NH}_3$  is depleted to less than  $10^{-10}$  at the surface.  $\text{H}_2\text{O}$  is below the 2- $\sigma$  upper limit due to cold trapping. If the temperature of the atmosphere near the cold trap was decreased or increased, then  $\text{H}_2\text{O}$  would correspondingly decrease or increase.

In contrast to W24, we find that an uninhabited Hycean scenario cannot be entirely ruled out by the data. A large number of factors effect the  $\text{CH}_4$  abundance, including the surface pressure, UV albedo, and the abundance of other molecules, such as sulfur bearing species, all of which have no observational constraints at

present. The choice of initial conditions instead determines the final result (as found previously in e.g., Hu et al. 2021; Madhusudhan et al. 2023a). We note that the plausibility of this scenario also depends on the temperature profile and whether a temperate surface ocean is actually physically possible for the assumed conditions.

Additionally, the destruction of  $\text{CH}_4$  is due to photodissociation, which does not occur on the nightside of a tidally locked exoplanet. Tsai et al. (2021a) used the 2D version of VULCAN to simulate a 1 bar  $\text{H}_2$ -rich atmosphere. Without winds,  $\text{CH}_4$  was depleted on the dayside when compared to the nightside, homogenising to an intermediate value with winds. If this qualitative result holds for a variety of conditions, then multidimensional models may be required to explain how  $\text{CH}_4$  can match the abundances at the terminator in an uninhabited Hycean scenario if the UV albedo is not otherwise high enough to stop significant dayside  $\text{CH}_4$  destruction.

#### 4.2.3. Inhabited Hycean scenario

The inhabited Hycean scenario assumes a biogenic source of  $\text{CH}_4$  on K2-18 b, e.g. through methanogenesis, as well as the consumption of CO. Several stud-

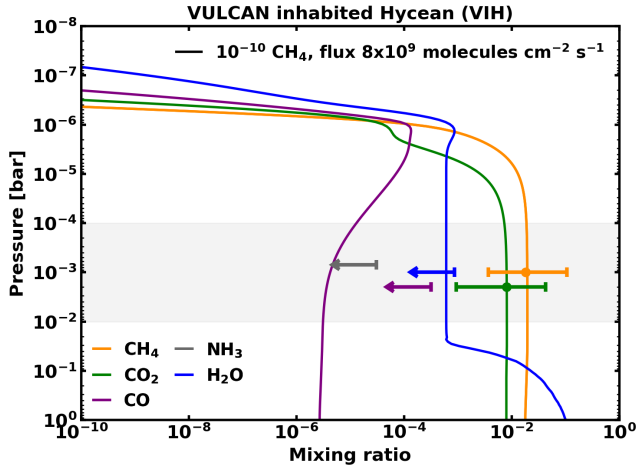


**Figure 8.** Inhabited Hycean scenario for K2-18 b using VULCAN. The GJ 176 spectrum with a 0.3 top of atmosphere albedo is used, as in W24, with the same  $P$ - $T$  and  $K_{zz}$  profile from W24. The inhabited hycean scenarios imposes a flux for  $\text{CH}_4$  at the planetary surface of  $8 \times 10^9$  molecules  $\text{cm}^{-2}$ . The inhabited simulation starts with a  $\text{CH}_4$  volume mixing ratio of  $10^{-10}$ .  $\text{CO}_2$  has a fixed mixing ratio condition at the surface of  $8 \times 10^{-3}$ . The mixing ratio of  $\text{CH}_4$ ,  $\text{CO}_2$ ,  $\text{CO}$ ,  $\text{H}_2\text{O}$ , and  $\text{NH}_3$  are plotted against atmospheric pressure. The constraints and colours are the same as in Fig. 1. This inhabited Hycean scenario is consistent with the retrieved abundance constraints from JWST observations (Madhusudhan et al. 2023b) for all five molecules, similar to the W24 inhabited Hycean scenario.

ies have suggested the possibility of such a  $\text{CH}_4$  source on K2-18 b (Madhusudhan et al. 2023a,b; Wogan et al. 2024; Glein 2024; Tsai et al. 2024a). We recreate a similar experiment to the W24 inhabited Hycean case using VULCAN (instead of Photochem used by W24) and show the results in Fig. 8. We use the same  $P$ - $T$  profile, stellar input spectrum, surface pressure, and fixed mixing ratios at the lower boundary. We initialise  $\text{CH}_4$  at a volume mixing ratio of  $10^{-10}$ .

To produce 2%  $\text{CH}_4$  by volume in the atmospheric simulation, we find a flux of  $8 \times 10^9$  molecules  $\text{cm}^{-2} \text{s}^{-1}$  using VULCAN, compared to the  $5 \times 10^{10}$  molecules  $\text{cm}^{-2} \text{s}^{-1}$  found in W24. Considering that Earth’s modern biogenic flux is  $\sim 1 \times 10^{11}$  molecules  $\text{cm}^{-2} \text{s}^{-1}$  (Jackson et al. 2020), and the surface of a Hycean world would be fully covered in an ocean, such a biogenic flux is not implausible.

Given a set of initial conditions, provided that the  $\text{CH}_4$  flux is sufficient to produce the observed  $\text{CH}_4$ , the inhabited Hycean scenario can be shown to be consistent with retrieved abundances. Alternatively, as shown in the previous section, an uninhabited Hycean atmosphere could also explain the  $\text{CH}_4$  abundance under some circumstances. However, even if a biogenic source of  $\text{CH}_4$  is not required to explain the data the possibility of life cannot be excluded. Moreover, the “inhabited Hycean” scenario can be thought of as an uninhabited Hycean which has an unknown source of  $\text{CH}_4$  and/or an unknown sink of CO.

## 5. SUMMARY AND DISCUSSION

In this study we presented a detailed exploration of photochemical models to investigate different scenarios for the temperate sub-Neptune K2-18 b. Here we summarise our results and discuss the implications. We first provide a summary of the key results presented in this study and how they compare to the results in W24. Subsequently, we describe the implications of our work for future studies and observations of exoplanetary atmospheres.

### 5.1. Summary

Following the photochemical modeling work of W24, we simulated the atmosphere of K2-18 b, assuming that it is either a Hycean world or a mini-Neptune with a deep atmosphere. With the results from Rigby et al. (2024) that discussed the issues with the magma ocean scenario for K2-18 b (Shorttle et al. 2024), and the lack of photochemical modelling in the supercritical ocean scenario (Luu et al. 2024), we have assessed the remaining three proposed scenarios: uninhabited Hycean, inhabited Hycean, and mini-Neptune.



The mini-Neptune scenario with current modelling from this study and three different studies (Wogan et al. 2024; Yang & Hu 2024a; Huang et al. 2024) is unable to explain the JWST data because the predicted abundances of between 2–4 molecules are incompatible with the observed constraints. Depending on the initial assumptions, either CO or CH<sub>4</sub>, or both molecules, are inconsistent with the abundance constraints in the uninhabited Hycean scenario. However, with a high enough surface pressure (e.g. 25 bar), a significant UV albedo of  $\approx 0.85$  (and/or the case where the GJ 176, GJ 436, and GJ 849 spectra overestimate the UV flux of K2-18), then the uninhabited Hycean can explain the abundances, and the presence of a biosphere is not required in that scenario. Moreover, if the age of K2-18 b is on the lower end of the age estimate ( $2.4 \pm 0.6$  Gyr), then the  $\approx 3.2$  Gyr simulations we performed in VULCAN may have overestimated CH<sub>4</sub> depletion. The inhabited Hycean scenario fits all five of the observational abundance constraints.

Whilst existing observations indicate there may be some clouds/hazes at the terminator for K2-18 b (Madhusudhan et al. 2023b), the albedo remains unconstrained, although the required planetary Bond albedo for a Hycean with a habitable ocean currently cannot be ruled out. Updated photochemical reaction networks, and 2D or 3D photochemical models, may produce mixing ratios that are compatible with observations for other scenarios. Future results from JWST observations are likely to narrow the constraints we have for the molecules in question (e.g., JWST C1 GO 2372; PI: Renyu Hu, JWST C1 GO 2722; PI: Nikku Madhusudhan).

Based on current observations and photochemical modelling, we now summarise the implications of our work:

- In contrast to W24, we find that both uninhabited and inhabited Hycean scenarios can explain the retrieved JWST abundances for K2-18 b given specific model assumptions. Future observations and photochemical simulations may favour a scenario different to a Hycean exoplanet, but existing observations and photochemical results currently support one of the Hycean scenarios. The mini-Neptune scenario of W24, using two independent 1D photochemical models, is inconsistent with retrieved mixing ratios over a range of initial conditions and sensitivity tests.
- Using inaccurate cross sections can modify the predicted abundance of key molecules (e.g. NH<sub>3</sub>, CO, CH<sub>4</sub>, SO<sub>2</sub>) by factors of up to  $\sim 10^3$  and

$\sim 10^9$  for Hycean and mini-Neptune scenarios, respectively. Different assumed photolysis branching ratios, which were not tested over a large parameter space here, are also likely to alter chemical predictions.

- Choosing only one stellar spectrum when modeling a planet with unknown incoming UV flux introduces further uncertainties, adding additional uncertainty when combined with different cross sections. We call for the spectrum of K2-18 to be measured with the Hubble Space Telescope. Until then, modellers should explore different stellar input spectra.

### 5.2. Which star represents K2-18?

The UV spectrum of K2-18 is unknown. Photochemical models of K2-18 b have thus far used observed spectra from other stars that are seemingly representative of K2-18 due to comparable measured stellar properties (e.g. radius,  $T_{\text{eff}}$ , and rotation rate). In the Hycean and mini-Neptune simulations, we used three stellar spectra that, under the assumption of stellar proxies, can be substituted for the stellar spectrum of K2-18. These were the MUSCLES spectra for GJ 176, GJ 436, and GJ 849, which are given with fractional uncertainties of up to  $\sim 10^3 - 10^4$  for the observed flux density. Out of all available spectra, it is possible that either GJ 176, or GJ 436, or GJ 849, does best represent K2-18. But this is not a certainty, and thus represents a general problem in accurately modeling exoplanet atmospheres. Furthermore, how the star and planetary atmosphere evolves through time is an important question regarding the current atmospheres we are able to observe with JWST.

Then there is the separate problem of stellar activity and flares, which are known to impact photochemistry in terrestrial atmospheres. When modeling terrestrial exoplanet atmospheres using a 3D model, Chen et al. (2021) found that frequent flaring reduces O<sub>3</sub> on K and M dwarf exoplanets, whilst Ridgway et al. (2023) found the opposite for a terrestrial Proxima Centauri b: flaring increased atmospheric O<sub>3</sub> by 20 times. Note that many of the assumptions in these two models were not the same. However, this does raise the question of whether such opposite predictions could occur for photochemically active species in temperate sub-Neptune atmospheres when using different photochemical models. The impact of flares on Hycean atmospheres remains untested and we leave that for future investigations.

### 5.3. Cross sections and branching ratios

Cross sections and branching ratios are key inputs to photochemical models which influence the vertical profile of many chemical species. As demonstrated by W24, a seemingly small change to a branching ratio for H<sub>2</sub>O photolysis at a single wavelength (Lyman- $\alpha$ ), can result in a big change for a specific molecule, like CH<sub>4</sub>. Similarly here, Fig. B2 shows large differences in branching ratios between models for multiple key species, and alongside discrepant cross sections (see Fig. B1), this may result in further uncertainties depending on the model and the chemical network.

As an initial test, we swapped the branching ratios from VULCAN into the standard W24 mini-Neptune setup (GJ 176, M/H = 100) for CO<sub>2</sub>, CH<sub>4</sub>, NH<sub>3</sub>, SO<sub>2</sub>, and O<sub>3</sub> and performed simulations with the Photochem and VULCAN binned and native cross sections. The largest perturbation observed in the photosphere was in the VULCAN native cross section case, where NH<sub>3</sub> and SO<sub>2</sub> decreased in the photosphere by up to a factor of 1100 and 900, respectively.

In simulations of terrestrial planetary atmospheres, the extended H<sub>2</sub>O cross sections, as recommended in Ranjan et al. (2020), impacted H<sub>2</sub>O mixing ratios and that of OH. Subsequently, Broussard et al. (2024) showed that for anoxic (lack of oxygen) terrestrial exoplanets orbiting FGKM host stars, the extended cross sections were the least important for M dwarf stars. Because Photochem does not use the recommended cross sections from Ranjan et al. (2020), this implies that the results we present may have even greater implications for Hycean and mini-Neptune exoplanets orbiting FGK stars, but that hypothesis must be tested.

Alternative chemical networks to those used here may change the results and conclusions of our work. For instance, there may be a mechanism which is able to replenish CH<sub>4</sub> in a Hycean atmosphere, or where CO and NH<sub>3</sub> are depleted in a mini-Neptune atmosphere.

Awareness of the impact of different assumptions and chemical input data sources is vital; having accurate and updated chemical input data is important for future interpretation of planetary spectra, and may influence whether a biosignature is attributed to a biogenic or abiogenic source.

#### 5.4. Implications for other planetary interpretation

It is important to consider how photochemical codes respond to different input data and initial conditions, because this can affect interpretations of other planetary spectra beyond K2-18 b. Recently, TOI-270 d was observed by JWST and the observations were analysed by two different groups (Benneke et al. 2024; Holmberg & Madhusudhan 2024, GO Program 4098). Both analyses

found evidence for CO<sub>2</sub> and CH<sub>4</sub> similar in abundance to K2-18 b, evidence for H<sub>2</sub>O, and weak evidence for CS<sub>2</sub>, a possible biosignature (Seager et al. 2013; Schweterman et al. 2018). Benneke et al. (2024) also report a possible signature of SO<sub>2</sub>, which Holmberg & Madhusudhan (2024) did not find. Neither studies detected NH<sub>3</sub> or CO, similar to the K2-18 b observations.

Holmberg & Madhusudhan (2024) report that the simultaneous detection of CH<sub>4</sub> and CO<sub>2</sub>, without the detection of NH<sub>3</sub>, lends weight to the argument that TOI-270 d could be a Hycean exoplanet. On the other hand, Benneke et al. (2024) argued that their abundance constraints for the atmosphere of TOI-270 d can be explained by a “Miscible-Envelope Sub-Neptune” exoplanet. To support their argument, Benneke et al. (2024) adapted the mini-Neptune setup of W24 to TOI-270 d, assuming a metallicity of 230 $\times$  solar and retaining the stellar spectrum to be of GJ 176. They claim the model abundances match the retrieved constraints for H<sub>2</sub>O, CO, CO<sub>2</sub>, NH<sub>3</sub>, and CH<sub>4</sub>. However, we find that those abundances are incompatible with the retrieved abundance constraints of Holmberg & Madhusudhan (2024) for CO, CH<sub>4</sub>, and H<sub>2</sub>O, for the “One offset + DT” case. Secondly, including different cross sections for TOI-270 d as we have here would affect NH<sub>3</sub> photolysis and impact its observability, because the pressure at which the NH<sub>3</sub> mixing ratio starts to decrease can change by a factor of  $\sim 100$ . Benneke et al. (2024) find weak evidence for SO<sub>2</sub> in the atmosphere of TOI-270 d, but don’t show the SO<sub>2</sub> mixing ratio in their figure 10 when simulating TOI-270 d with Photochem. Again, using different cross sections would change their predicted SO<sub>2</sub> mixing ratio.

Benneke et al. (2024) state that their atmospheric simulation of TOI-270 d using the model EPACRIS (Yang & Hu 2024b) does produce the right CO<sub>2</sub>, H<sub>2</sub>O, CH<sub>4</sub>, and SO<sub>2</sub> mixing ratios, but it is unclear if EPACRIS predicts concentrations for other molecules (CO and NH<sub>3</sub>) that are consistent with the retrieved constraints as those results are not reported. Their modeling finds much lower CS<sub>2</sub> mixing ratios ( $10^{-10}$  near 1 mbar) than the tentatively detected abundance of CS<sub>2</sub> ( $\approx 3 \times 10^{-4}$  at  $2.55\sigma$ ). Finally, it is arguable that the star GJ 163 better represents the host star TOI 270 more than GJ 176 (see Appendix C and Table C1); using GJ 163 may influence the results presented in Benneke et al. (2024).

#### 5.5. Tidally locked anisotropy

When exoplanets pass in front of their host stars, transmission spectra of their atmospheres can be taken to reveal absorption signatures from any chemical species present. Transmission spectra probe the ter-

minator region of an exoplanet’s atmosphere. Photochemical modeling in 1D may not adequately capture this portion of the atmosphere. 3D modeling of terrestrial exoplanets that are tidally locked have shown that photochemically active molecules can be distributed inhomogeneously (Proedrou & Hocke 2016; Cooke et al. 2023; Braam et al. 2023), including at orbital periods longer than K2-18 b (Chen et al. 2018, 2019), where DMS showed large day-to-nightside anisotropy (Chen et al. 2018). Similarly for larger exoplanets such as hot Jupiters, 2D and 3D models are critical for understanding chemical anisotropy and explaining observed spectra (Steinrueck et al. 2019; Tsai et al. 2022; Lee et al. 2023; Steinrueck et al. 2023; Tsai et al. 2023, 2024b; Espinoza et al. 2024). There is no reason to expect that temperate sub-Neptunes, including mini-Neptunes and Hycean exoplanets, would be any different.

Our results in section 4.2.2 regarding an uninhabited Hycean scenario showed that pressures of tens of bar and an adequate UV albedo (e.g. 0.75) may be necessary to prevent substantial CH<sub>4</sub> depletion below the abundance constraint for K2-18 b (~1% by volume). Nevertheless, a 25 bar Hycean world with a habitable ocean could be physically infeasible due to a steam runaway greenhouse (Scheucher et al. 2020; Innes et al. 2023; Pierrehumbert 2023; Leconte et al. 2024). The abundance of CH<sub>4</sub> in a case with a shallower ocean surface (e.g., 10 bar) will be dependent on many free model parameters that are not constrained, which include: the UV flux of the host star, the albedo (both Bond and UV), the efficiency of CH<sub>4</sub> recycling on the nightside of a tidally locked exoplanet, and the age of K2-18 b. Further explorations into such a parameter space demand the use of multi-dimensional models to comprehensively assess the efficacy of the uninhabited Hycean scenario for K2-18 b, and other Hycean candidates such as TOI-270 d.

### 5.6. Methane as a biosignature

In the context of a potentially habitable exoplanet, a molecule present in the exoplanet’s atmosphere that indicates biological activity can be considered a biosignature (Grenfell 2017; Meadows et al. 2018; Schwieterman & Leung 2024).

CH<sub>4</sub> is a molecule on Earth that has both abiotic and biotic sources. In an atmosphere composed primarily of reducing gasses (e.g. H<sub>2</sub>), similar to the weakly reducing conditions expected during the Archean eon (4 - 2.4 Gyr ago) on Earth (Catling et al. 2001; Kasting 2005; Catling & Zahnle 2020), methanogenesis could add significant quantities of CH<sub>4</sub> to the atmosphere.

On an Earth-like rocky exoplanet, the atmospheric combination of CO<sub>2</sub> and CH<sub>4</sub>, with a lack of CO,

is thought to be a possible biosignature (Krissansen-Totton et al. 2018, 2019). False positives of this combination in rocky exoplanetary atmospheres may be improbable (Wogan et al. 2020; Thompson et al. 2022). However, on rocky exoplanets with H<sub>2</sub> dominated atmospheres, CH<sub>4</sub> is not an unambiguous sign of life because it can be produced through photochemistry or geochemistry (Seager et al. 2013). Such geochemical sources consist of serpentinizing reactions and magmatic outgassing (Thompson et al. 2022), and these processes are not expected to occur on ocean and Hycean worlds (Kite et al. 2009; Kite & Ford 2018; Madhusudhan et al. 2023a).

Given all the simulations here, and those that exist within the literature, the inhabited Hycean fits the observations best, followed by the uninhabited Hycean, while the mini-Neptune is more difficult to reconcile with observations. It is therefore pertinent to consider whether the observed CH<sub>4</sub> in the atmosphere of K2-18 b might be from a biological source.

Previous studies have argued that CH<sub>4</sub> could be produced by extraterrestrial life on Hycean worlds (Madhusudhan et al. 2023a,b; Wogan et al. 2024; Glein 2024; Tsai et al. 2024a) and thus considered a potential biosignature in the context of a habitable environment. Despite this, the relative proportions of possible biotic versus abiotic sources in a Hycean environment is not well understood and requires further exploration. If K2-18 b is a Hycean exoplanet, whether it is viable to disentangle the ambiguity of the CH<sub>4</sub> source remains an open question, and other lines of evidence will likely be necessary to determine if the planet is inhabited, rather than just habitable.

Overall, the interpretation of atmospheric observations using photochemical models of an exoplanet atmosphere depends on various factors, including the initial conditions, the boundary conditions, the number of dimensions included, and the input parameters such as chemical reaction rates, photochemical cross sections, and the assumed stellar spectrum. Therefore, conclusions drawn from JWST exoplanet atmospheric observations should be aware of the many uncertainties that exist in photochemical codes (e.g. cross sections), stellar spectrum inputs (MUSCLES observations and synthetic spectra), and be cautious when not including 3D effects, because transmission spectra probe the exoplanet’s terminator. Such critical assessment is necessary now that astronomers have started to observe potentially habitable exoplanet atmospheres.

### ACKNOWLEDGMENTS

We thank the anonymous reviewers for their valuable comments. We thank Nick Wogan, the Atmos team,

and Shami Tsai, for making their models *Photochem*, *Atmos*, and *VULCAN*, respectively, publicly available on GitHub. GC thanks Nicholas Wogan and Shami Tsai for

useful advice regarding modeling with *VULCAN*, Lalitha Sairam and Måns Holmberg for helpful discussions, and Savvas Constantinou for advice and guidance with modeling.

## REFERENCES

- Abe, Y., Abe-Ouchi, A., Sleep, N. H., & Zahnle, K. J. 2011, *Astrobiology*, 11, 443, doi: [10.1089/ast.2010.0545](https://doi.org/10.1089/ast.2010.0545)
- Arney, G. N., Meadows, V. S., Domagal-Goldman, S. D., et al. 2017, *ApJ*, 836, 49, doi: [10.3847/1538-4357/836/1/49](https://doi.org/10.3847/1538-4357/836/1/49)
- Batalha, N. E., Marley, M. S., Lewis, N. K., & Fortney, J. J. 2019, *ApJ*, 878, 70, doi: [10.3847/1538-4357/ab1b51](https://doi.org/10.3847/1538-4357/ab1b51)
- Benneke, B., Werner, M., Petigura, E., et al. 2017, *ApJ*, 834, 187, doi: [10.3847/1538-4357/834/2/187](https://doi.org/10.3847/1538-4357/834/2/187)
- Benneke, B., Wong, I., Piaulet, C., et al. 2019, *ApJL*, 887, L14, doi: [10.3847/2041-8213/ab59dc](https://doi.org/10.3847/2041-8213/ab59dc)
- Benneke, B., Roy, P.-A., Coulombe, L.-P., et al. 2024, arXiv e-prints, arXiv:2403.03325. <https://arxiv.org/abs/2403.03325>
- Bonfils, X., Mayor, M., Delfosse, X., et al. 2007, *A&A*, 474, 293, doi: [10.1051/0004-6361:20077068](https://doi.org/10.1051/0004-6361:20077068)
- Bonfils, X., Delfosse, X., Udry, S., et al. 2013, *A&A*, 549, A109, doi: [10.1051/0004-6361/201014704](https://doi.org/10.1051/0004-6361/201014704)
- Bourrier, V., Lovis, C., Beust, H., et al. 2018, *Nature*, 553, 477, doi: [10.1038/nature24677](https://doi.org/10.1038/nature24677)
- Braam, M., Palmer, P. I., Decin, L., Cohen, M., & Mayne, N. J. 2023, *MNRAS*, 526, 263, doi: [10.1093/mnras/stad2704](https://doi.org/10.1093/mnras/stad2704)
- Broussard, W., Schwieterman, E. W., Ranjan, S., et al. 2024, *ApJ*, 967, 114, doi: [10.3847/1538-4357/ad3a65](https://doi.org/10.3847/1538-4357/ad3a65)
- Brown, A., Schneider, P. C., France, K., et al. 2023, *AJ*, 165, 195, doi: [10.3847/1538-3881/acc38a](https://doi.org/10.3847/1538-3881/acc38a)
- Butler, R. P., Johnson, J. A., Marcy, G. W., et al. 2006, *PASP*, 118, 1685, doi: [10.1086/510500](https://doi.org/10.1086/510500)
- Catling, D. C., & Zahnle, K. J. 2020, *Science Advances*, 6, eaax1420, doi: [10.1126/sciadv.aax1420](https://doi.org/10.1126/sciadv.aax1420)
- Catling, D. C., Zahnle, K. J., & McKay, C. P. 2001, *Science*, 293, 839, doi: [10.1126/science.1061976](https://doi.org/10.1126/science.1061976)
- Chen, H., Wolf, E. T., Kopparapu, R., Domagal-Goldman, S., & Horton, D. E. 2018, *ApJL*, 868, L6, doi: [10.3847/2041-8213/aaedb2](https://doi.org/10.3847/2041-8213/aaedb2)
- Chen, H., Wolf, E. T., Zhan, Z., & Horton, D. E. 2019, *ApJ*, 886, 16, doi: [10.3847/1538-4357/ab4f7e](https://doi.org/10.3847/1538-4357/ab4f7e)
- Chen, H., Zhan, Z., Youngblood, A., et al. 2021, *Nature Astronomy*, 5, 298, doi: [10.1038/s41550-020-01264-1](https://doi.org/10.1038/s41550-020-01264-1)
- Cooke, G. J., Marsh, D. R., Walsh, C., & Youngblood, A. 2023, *ApJ*, 959, 45, doi: [10.3847/1538-4357/ad0381](https://doi.org/10.3847/1538-4357/ad0381)
- Correia, A. C. M., Couetdic, J., Laskar, J., et al. 2010, *A&A*, 511, A21, doi: [10.1051/0004-6361/200912700](https://doi.org/10.1051/0004-6361/200912700)
- Crossfield, I. J. M., Dragomir, D., Cowan, N. B., et al. 2020, *ApJL*, 903, L7, doi: [10.3847/2041-8213/abbc71](https://doi.org/10.3847/2041-8213/abbc71)
- Espinoza, N., Steinrueck, M. E., Kirk, J., et al. 2024, *Nature*, 632, 1017, doi: [10.1038/s41586-024-07768-4](https://doi.org/10.1038/s41586-024-07768-4)
- Forveille, T., Bonfils, X., Delfosse, X., et al. 2009, *A&A*, 493, 645, doi: [10.1051/0004-6361:200810557](https://doi.org/10.1051/0004-6361:200810557)
- France, K., Loyd, R. O. P., Youngblood, A., et al. 2016, *ApJ*, 820, 89, doi: [10.3847/0004-637X/820/2/89](https://doi.org/10.3847/0004-637X/820/2/89)
- Froning, C. S., Kowalski, A., France, K., et al. 2019, *ApJL*, 871, L26, doi: [10.3847/2041-8213/aaffcd](https://doi.org/10.3847/2041-8213/aaffcd)
- Fulton, B. J., & Petigura, E. A. 2018, *AJ*, 156, 264, doi: [10.3847/1538-3881/aae828](https://doi.org/10.3847/1538-3881/aae828)
- Fulton, B. J., Petigura, E. A., Howard, A. W., et al. 2017, *AJ*, 154, 109, doi: [10.3847/1538-3881/aa80eb](https://doi.org/10.3847/1538-3881/aa80eb)
- Glein, C. R. 2024, *ApJL*, 964, L19, doi: [10.3847/2041-8213/ad3079](https://doi.org/10.3847/2041-8213/ad3079)
- Grenfell, J. L. 2017, *PhR*, 713, 1, doi: [10.1016/j.physrep.2017.08.003](https://doi.org/10.1016/j.physrep.2017.08.003)
- Guinan, E. F., & Engle, S. G. 2019, *Research Notes of the American Astronomical Society*, 3, 189, doi: [10.3847/2515-5172/ab6086](https://doi.org/10.3847/2515-5172/ab6086)
- Günther, M. N., Pozuelos, F. J., Dittmann, J. A., et al. 2019, *Nature Astronomy*, 3, 1099, doi: [10.1038/s41550-019-0845-5](https://doi.org/10.1038/s41550-019-0845-5)
- Hawley, S. L., Gizis, J. E., & Reid, I. N. 1996, *AJ*, 112, 2799, doi: [10.1086/118222](https://doi.org/10.1086/118222)
- Holmberg, M., & Madhusudhan, N. 2024, *A&A*, 683, L2, doi: [10.1051/0004-6361/202348238](https://doi.org/10.1051/0004-6361/202348238)
- Hoyer, S., Jenkins, J. S., Parmentier, V., et al. 2023, *A&A*, 675, A81, doi: [10.1051/0004-6361/202346117](https://doi.org/10.1051/0004-6361/202346117)
- Hu, R. 2021, *ApJ*, 921, 27, doi: [10.3847/1538-4357/ac1789](https://doi.org/10.3847/1538-4357/ac1789)
- Hu, R., Damiano, M., Scheucher, M., et al. 2021, *ApJL*, 921, L8, doi: [10.3847/2041-8213/ac1f92](https://doi.org/10.3847/2041-8213/ac1f92)
- Hu, R., Gaillard, F., & Kite, E. S. 2023, *ApJL*, 948, L20, doi: [10.3847/2041-8213/acd0b4](https://doi.org/10.3847/2041-8213/acd0b4)
- Huang, Z., Yu, X., Tsai, S.-M., et al. 2024, arXiv e-prints, arXiv:2407.09009, doi: [10.48550/arXiv.2407.09009](https://doi.org/10.48550/arXiv.2407.09009)
- Ibañez Bustos, R. V., Buccino, A. P., Messina, S., Lanza, A. F., & Mauas, P. J. D. 2020, *A&A*, 644, A2, doi: [10.1051/0004-6361/202039164](https://doi.org/10.1051/0004-6361/202039164)

- Innes, H., Tsai, S.-M., & Pierrehumbert, R. T. 2023, *ApJ*, 953, 168, doi: [10.3847/1538-4357/ace346](https://doi.org/10.3847/1538-4357/ace346)
- Irwin, P. G. J., Toledo, D., Braude, A. S., et al. 2019, *Icarus*, 331, 69, doi: [10.1016/j.icarus.2019.05.011](https://doi.org/10.1016/j.icarus.2019.05.011)
- Irwin, P. G. J., Teanby, N. A., Fletcher, L. N., et al. 2022, *Journal of Geophysical Research (Planets)*, 127, e07189, doi: [10.1029/2022JE007189](https://doi.org/10.1029/2022JE007189)
- Irwin, P. G. J., Dobinson, J., James, A., et al. 2023, *Journal of Geophysical Research (Planets)*, 128, e2023JE007980, doi: [10.1029/2023JE007980](https://doi.org/10.1029/2023JE007980)
- Jackson, R. B., Sauniois, M., Bousquet, P., et al. 2020, *Environmental Research Letters*, 15, 071002, doi: [10.1088/1748-9326/ab9ed2](https://doi.org/10.1088/1748-9326/ab9ed2)
- Kasting, J. 2005, *Precambrian Research*, 137, 119, doi: [10.1016/j.precamres.2005.03.002](https://doi.org/10.1016/j.precamres.2005.03.002)
- Kasting, J. F., Holland, H. D., & Pinto, J. P. 1985, *J. Geophys. Res.*, 90, 10,497, doi: [10.1029/JD090iD06p10497](https://doi.org/10.1029/JD090iD06p10497)
- Kasting, J. F., Whitmire, D. P., & Reynolds, R. T. 1993, *Icarus*, 101, 108, doi: [10.1006/icar.1993.1010](https://doi.org/10.1006/icar.1993.1010)
- Kempton, E. M. R., Zhang, M., Bean, J. L., et al. 2023, *Nature*, 620, 67, doi: [10.1038/s41586-023-06159-5](https://doi.org/10.1038/s41586-023-06159-5)
- Kharecha, P., Kasting, J., & Siefert, J. 2005, *Geobiology*, 3, 53, doi: [10.1111/j.1472-4669.2005.00049.x](https://doi.org/10.1111/j.1472-4669.2005.00049.x)
- Kiraga, M., & Stepien, K. 2007, *AcA*, 57, 149, doi: [10.48550/arXiv.0707.2577](https://doi.org/10.48550/arXiv.0707.2577)
- Kirkpatrick, J. D., Henry, T. J., & McCarthy, Donald W., J. 1991, *ApJS*, 77, 417, doi: [10.1086/191611](https://doi.org/10.1086/191611)
- Kite, E. S., & Ford, E. B. 2018, *ApJ*, 864, 75, doi: [10.3847/1538-4357/aad6e0](https://doi.org/10.3847/1538-4357/aad6e0)
- Kite, E. S., Manga, M., & Gaidos, E. 2009, *ApJ*, 700, 1732, doi: [10.1088/0004-637X/700/2/1732](https://doi.org/10.1088/0004-637X/700/2/1732)
- Kitzmann, D., Stock, J. W., & Patzer, A. B. C. 2024, *MNRAS*, 527, 7263, doi: [10.1093/mnras/stad3515](https://doi.org/10.1093/mnras/stad3515)
- Kopparapu, R. k., Wolf, E. T., Haqq-Misra, J., et al. 2016, *ApJ*, 819, 84, doi: [10.3847/0004-637X/819/1/84](https://doi.org/10.3847/0004-637X/819/1/84)
- Kopparapu, R. K., Ramirez, R., Kasting, J. F., et al. 2013, *ApJ*, 765, 131, doi: [10.1088/0004-637X/765/2/131](https://doi.org/10.1088/0004-637X/765/2/131)
- Krissansen-Totton, J., Olson, S., & Catling, D. C. 2018, *Science Advances*, 4, eaao5747, doi: [10.1126/sciadv.aao5747](https://doi.org/10.1126/sciadv.aao5747)
- Krissansen-Totton, J., Arney, G. N., Catling, D. C., et al. 2019, *BAAS*, 51, 158
- Lecante, J., Spiga, A., Clément, N., et al. 2024, *A&A*, 686, A131, doi: [10.1051/0004-6361/202348928](https://doi.org/10.1051/0004-6361/202348928)
- Lee, E. K. H., Tsai, S.-M., Hammond, M., & Tan, X. 2023, *A&A*, 672, A110, doi: [10.1051/0004-6361/202245473](https://doi.org/10.1051/0004-6361/202245473)
- Li, L., Jiang, X., West, R., et al. 2018, *Nature Communications*, 9, 3709
- Lichtenberg, T., & Miguel, Y. 2024, arXiv e-prints, arXiv:2405.04057, doi: [10.48550/arXiv.2405.04057](https://doi.org/10.48550/arXiv.2405.04057)
- Linsky, J. L., Wood, B. E., Youngblood, A., et al. 2020, *ApJ*, 902, 3, doi: [10.3847/1538-4357/abb36f](https://doi.org/10.3847/1538-4357/abb36f)
- Loftus, K., Wordsworth, R. D., & Morley, C. V. 2019, *ApJ*, 887, 231, doi: [10.3847/1538-4357/ab58cc](https://doi.org/10.3847/1538-4357/ab58cc)
- Lopez, E. D., & Fortney, J. J. 2014, *ApJ*, 792, 1, doi: [10.1088/0004-637X/792/1/1](https://doi.org/10.1088/0004-637X/792/1/1)
- Loyd, R. O. P., France, K., Youngblood, A., et al. 2016, *ApJ*, 824, 102, doi: [10.3847/0004-637X/824/2/102](https://doi.org/10.3847/0004-637X/824/2/102)
- Loyd, R. O. P., Shkolnik, E. L., Schneider, A. C., et al. 2021, *ApJ*, 907, 91, doi: [10.3847/1538-4357/abd0f0](https://doi.org/10.3847/1538-4357/abd0f0)
- Luque, R., & Pallé, E. 2022, *Science*, 377, 1211, doi: [10.1126/science.abl7164](https://doi.org/10.1126/science.abl7164)
- Luu, C. N., Yu, X., Glein, C. R., et al. 2024, arXiv e-prints, arXiv:2409.06258, doi: [10.48550/arXiv.2409.06258](https://doi.org/10.48550/arXiv.2409.06258)
- Madhusudhan, N., Moses, J. I., Rigby, F., & Barrier, E. 2023a, *Faraday Discussions*, 245, 80, doi: [10.1039/D3FD00075C](https://doi.org/10.1039/D3FD00075C)
- Madhusudhan, N., Nixon, M. C., Welbanks, L., Piette, A. A., & Booth, R. A. 2020, *ApJL*, 891, L7, doi: [10.3847/2041-8213/ab7229](https://doi.org/10.3847/2041-8213/ab7229)
- Madhusudhan, N., Piette, A. A., & Constantinou, S. 2021, *ApJ*, 918, 1, doi: [10.3847/1538-4357/abfd9c](https://doi.org/10.3847/1538-4357/abfd9c)
- Madhusudhan, N., Sarkar, S., Constantinou, S., et al. 2023b, *ApJL*, 956, L13, doi: [10.3847/2041-8213/acf577](https://doi.org/10.3847/2041-8213/acf577)
- Madhusudhan, N., & Seager, S. 2009, *ApJ*, 707, 24, doi: [10.1088/0004-637X/707/1/24](https://doi.org/10.1088/0004-637X/707/1/24)
- Meadows, V. S., Reinhard, C. T., Arney, G. N., et al. 2018, *Astrobiology*, 18, 630, doi: [10.1089/ast.2017.1727](https://doi.org/10.1089/ast.2017.1727)
- Mikal-Evans, T., Madhusudhan, N., Dittmann, J., et al. 2023, *AJ*, 165, 84, doi: [10.3847/1538-3881/aca90b](https://doi.org/10.3847/1538-3881/aca90b)
- Montet, B. T., Morton, T. D., Foreman-Mackey, D., et al. 2015, *ApJ*, 809, 25, doi: [10.1088/0004-637X/809/1/25](https://doi.org/10.1088/0004-637X/809/1/25)
- Mordasini, C., Alibert, Y., Klahr, H., & Henning, T. 2012, *A&A*, 547, A111, doi: [10.1051/0004-6361/201118457](https://doi.org/10.1051/0004-6361/201118457)
- Moutou, C., Delfosse, X., Petit, A. C., et al. 2023, *A&A*, 678, A207, doi: [10.1051/0004-6361/202346813](https://doi.org/10.1051/0004-6361/202346813)
- Mukherjee, S., Batalha, N. E., Fortney, J. J., & Marley, M. S. 2023, *ApJ*, 942, 71, doi: [10.3847/1538-4357/ac9f48](https://doi.org/10.3847/1538-4357/ac9f48)
- Nixon, M. C., & Madhusudhan, N. 2021, *MNRAS*, 505, 3414, doi: [10.1093/mnras/stab1500](https://doi.org/10.1093/mnras/stab1500)
- Noack, L., Höning, D., Rivoldini, A., et al. 2016, *Icarus*, 277, 215, doi: [10.1016/j.icarus.2016.05.009](https://doi.org/10.1016/j.icarus.2016.05.009)
- Pearl, J. C., & Conrath, B. J. 1991, *J. Geophys. Res.*, 96, 18921, doi: [10.1029/91JA01087](https://doi.org/10.1029/91JA01087)
- Pierrehumbert, R. T. 2023, *ApJ*, 944, 20, doi: [10.3847/1538-4357/acafdf](https://doi.org/10.3847/1538-4357/acafdf)
- Piette, A. A., & Madhusudhan, N. 2020, *ApJ*, 904, 154, doi: [10.3847/1538-4357/abfbf1](https://doi.org/10.3847/1538-4357/abfbf1)

- Pinamonti, M., Barbato, D., Sozzetti, A., et al. 2023, *A&A*, 677, A122, doi: [10.1051/0004-6361/202346476](https://doi.org/10.1051/0004-6361/202346476)
- Pineda, J. S., Youngblood, A., & France, K. 2021a, *ApJ*, 918, 40, doi: [10.3847/1538-4357/ac0aea](https://doi.org/10.3847/1538-4357/ac0aea)
- . 2021b, *ApJ*, 911, 111, doi: [10.3847/1538-4357/abe8d7](https://doi.org/10.3847/1538-4357/abe8d7)
- Proedrou, E., & Hocke, K. 2016, *Earth, Planets and Space*, 68, 96, doi: [10.1186/s40623-016-0461-x](https://doi.org/10.1186/s40623-016-0461-x)
- Ranjan, S., Schwieterman, E. W., Harman, C., et al. 2020, *ApJ*, 896, 148, doi: [10.3847/1538-4357/ab9363](https://doi.org/10.3847/1538-4357/ab9363)
- Ridgway, R. J., Zamyatina, M., Mayne, N. J., et al. 2023, *MNRAS*, 518, 2472, doi: [10.1093/mnras/stac3105](https://doi.org/10.1093/mnras/stac3105)
- Rigby, F. E., & Madhusudhan, N. 2024, *MNRAS*, 529, 409, doi: [10.1093/mnras/stae413](https://doi.org/10.1093/mnras/stae413)
- Rigby, F. E., Pica-Ciamarra, L., Holmberg, M., et al. 2024, arXiv preprint arXiv:2409.03683
- Robbins-Blanch, N., Kataria, T., Batalha, N. E., & Adams, D. J. 2022, *ApJ*, 930, 93, doi: [10.3847/1538-4357/ac658c](https://doi.org/10.3847/1538-4357/ac658c)
- Salz, M., Schneider, P. C., Czesla, S., & Schmitt, J. H. M. M. 2015, *A&A*, 576, A42, doi: [10.1051/0004-6361/201425243](https://doi.org/10.1051/0004-6361/201425243)
- Sarkis, P., Henning, T., Kürster, M., et al. 2018, *AJ*, 155, 257, doi: [10.3847/1538-3881/aac108](https://doi.org/10.3847/1538-3881/aac108)
- Scheucher, M., Wunderlich, F., Grenfell, J. L., et al. 2020, *ApJ*, 898, 44, doi: [10.3847/1538-4357/ab9084](https://doi.org/10.3847/1538-4357/ab9084)
- Schwieterman, E. W., & Leung, M. 2024, *Reviews in Mineralogy and Geochemistry*, 90, 465, doi: [10.2138/rmg.2024.90.13](https://doi.org/10.2138/rmg.2024.90.13)
- Schwieterman, E. W., Kiang, N. Y., Parenteau, M. N., et al. 2018, *Astrobiology*, 18, 663, doi: [10.1089/ast.2017.1729](https://doi.org/10.1089/ast.2017.1729)
- Seager, S., Bains, W., & Hu, R. 2013, *ApJ*, 777, 95, doi: [10.1088/0004-637X/777/2/95](https://doi.org/10.1088/0004-637X/777/2/95)
- Segura, A., Krelove, K., Kasting, J. F., et al. 2003, *Astrobiology*, 3, 689
- Shorttle, O., Jordan, S., Nicholls, H., Lichtenberg, T., & Bower, D. J. 2024, *ApJL*, 962, L8, doi: [10.3847/2041-8213/ad206e](https://doi.org/10.3847/2041-8213/ad206e)
- Steinrueck, M. E., Koskinen, T., Lavvas, P., et al. 2023, *ApJ*, 951, 117, doi: [10.3847/1538-4357/acd4bb](https://doi.org/10.3847/1538-4357/acd4bb)
- Steinrueck, M. E., Parmentier, V., Showman, A. P., Lothringer, J. D., & Lupu, R. E. 2019, *ApJ*, 880, 14, doi: [10.3847/1538-4357/ab2598](https://doi.org/10.3847/1538-4357/ab2598)
- Stock, J. W., Kitzmann, D., & Patzer, A. B. C. 2022, *MNRAS*, 517, 4070, doi: [10.1093/mnras/stac2623](https://doi.org/10.1093/mnras/stac2623)
- Stock, J. W., Kitzmann, D., Patzer, A. B. C., & Sedlmayr, E. 2018, *MNRAS*, 479, 865, doi: [10.1093/mnras/sty1531](https://doi.org/10.1093/mnras/sty1531)
- Suárez Mascareño, A., Rebolo, R., González Hernández, J. I., & Esposito, M. 2015, *MNRAS*, 452, 2745, doi: [10.1093/mnras/stv1441](https://doi.org/10.1093/mnras/stv1441)
- Thompson, M. A., Krissansen-Totton, J., Wogan, N., Telus, M., & Fortney, J. J. 2022, *Proceedings of the National Academy of Science*, 119, e2117933119, doi: [10.1073/pnas.2117933119](https://doi.org/10.1073/pnas.2117933119)
- Tsai, S.-M., Innes, H., Lichtenberg, T., et al. 2021a, *ApJL*, 922, L27, doi: [10.3847/2041-8213/ac399a](https://doi.org/10.3847/2041-8213/ac399a)
- Tsai, S.-M., Innes, H., Wogan, N. F., & Schwieterman, E. W. 2024a, *ApJL*, 966, L24, doi: [10.3847/2041-8213/ad3801](https://doi.org/10.3847/2041-8213/ad3801)
- Tsai, S.-M., Lee, E. K. H., & Pierrehumbert, R. 2022, *A&A*, 664, A82, doi: [10.1051/0004-6361/202142816](https://doi.org/10.1051/0004-6361/202142816)
- Tsai, S.-M., Lyons, J. R., Grosheintz, L., et al. 2017, *ApJS*, 228, 20, doi: [10.3847/1538-4365/228/2/20](https://doi.org/10.3847/1538-4365/228/2/20)
- Tsai, S.-M., Malik, M., Kitzmann, D., et al. 2021b, *ApJ*, 923, 264, doi: [10.3847/1538-4357/ac29bc](https://doi.org/10.3847/1538-4357/ac29bc)
- Tsai, S.-M., Lee, E. K. H., Powell, D., et al. 2023, *Nature*, 617, 483, doi: [10.1038/s41586-023-05902-2](https://doi.org/10.1038/s41586-023-05902-2)
- Tsai, S.-M., Parmentier, V., Mendonça, J. M., et al. 2024b, *ApJ*, 963, 41, doi: [10.3847/1538-4357/ad1600](https://doi.org/10.3847/1538-4357/ad1600)
- Tuomi, M., & Anglada-Escudé, G. 2013, *A&A*, 556, A111, doi: [10.1051/0004-6361/201321174](https://doi.org/10.1051/0004-6361/201321174)
- Valencia, D., Guillot, T., Parmentier, V., & Freedman, R. S. 2013, *ApJ*, 775, 10, doi: [10.1088/0004-637X/775/1/10](https://doi.org/10.1088/0004-637X/775/1/10)
- Van Eylen, V., Astudillo-Defru, N., Bonfils, X., et al. 2021, *MNRAS*, 507, 2154, doi: [10.1093/mnras/stab2143](https://doi.org/10.1093/mnras/stab2143)
- Van Trump, J. E., & Miller, S. L. 1973, *Earth and Planetary Science Letters*, 20, 145, doi: [10.1016/0012-821X\(73\)90152-0](https://doi.org/10.1016/0012-821X(73)90152-0)
- von Braun, K., Boyajian, T. S., Kane, S. R., et al. 2012, *ApJ*, 753, 171, doi: [10.1088/0004-637X/753/2/171](https://doi.org/10.1088/0004-637X/753/2/171)
- von Braun, K., Boyajian, T. S., van Belle, G. T., et al. 2014, *MNRAS*, 438, 2413, doi: [10.1093/mnras/stt2360](https://doi.org/10.1093/mnras/stt2360)
- Wilson, D. J., Froning, C. S., Duvvuri, G. M., et al. 2021, *ApJ*, 911, 18, doi: [10.3847/1538-4357/abe771](https://doi.org/10.3847/1538-4357/abe771)
- Windsor, J. D., Robinson, T. D., Kopparapu, R. k., et al. 2024, arXiv e-prints, arXiv:2401.12204, doi: [10.48550/arXiv.2401.12204](https://doi.org/10.48550/arXiv.2401.12204)
- Wogan, N., Krissansen-Totton, J., & Catling, D. C. 2020, *PSJ*, 1, 58, doi: [10.3847/PSJ/abb99e](https://doi.org/10.3847/PSJ/abb99e)
- Wogan, N. F., Batalha, N. E., Zahnle, K. J., et al. 2024, *ApJL*, 963, L7, doi: [10.3847/2041-8213/ad2616](https://doi.org/10.3847/2041-8213/ad2616)
- Wogan, N. F., Catling, D. C., Zahnle, K. J., & Claire, M. W. 2022, *Proceedings of the National Academy of Science*, 119, e2205618119, doi: [10.1073/pnas.2205618119](https://doi.org/10.1073/pnas.2205618119)
- Wogan, N. F., Catling, D. C., Zahnle, K. J., & Lupu, R. 2023, *PSJ*, 4, 169, doi: [10.3847/PSJ/aced83](https://doi.org/10.3847/PSJ/aced83)
- Yang, J., & Hu, R. 2024a, *ApJL*, 971, L48, doi: [10.3847/2041-8213/ad6b25](https://doi.org/10.3847/2041-8213/ad6b25)
- . 2024b, *ApJ*, 966, 189, doi: [10.3847/1538-4357/ad35c8](https://doi.org/10.3847/1538-4357/ad35c8)

Youngblood, A., France, K., Loyd, R. O. P., et al. 2016,  
ApJ, 824, 101, doi: [10.3847/0004-637X/824/2/101](https://doi.org/10.3847/0004-637X/824/2/101)

—. 2017, ApJ, 843, 31, doi: [10.3847/1538-4357/aa76dd](https://doi.org/10.3847/1538-4357/aa76dd)  
Yu, X., Moses, J. I., Fortney, J. J., & Zhang, X. 2021, ApJ,  
914, 38, doi: [10.3847/1538-4357/abfdc7](https://doi.org/10.3847/1538-4357/abfdc7)

## APPENDIX

## A. SIMULATIONS PERFORMED

We performed hundreds of simulations over the three scenarios, using both the W24 setup and the VULCAN 1D photochemical model. The simulations using the W24 setup are shown in Table A1, and those using VULCAN are shown in Table A2. We altered cross section sources and their wavelength resolution, as well as the stellar input spectrum in the W24 setup. See Appendix B for more information regarding photochemical cross sections and branching ratios. The three different stellar spectra used in the W24 setup were GJ 176, GJ 436, and GJ 849. GJ 176 and GJ 436 were used in VULCAN simulations. Appendix C details why these stars were chosen.

The boundary conditions are given in Table A1 and Table A2. If a boundary condition is not listed in these tables, then the molecule has a zero flux boundary condition. An exception to this is H<sub>2</sub>O, the abundance profile of which is based on the humidity and the  $P$ - $T$  profile.

For the W24 Hycean cases, we do not vary  $K_{zz}$ , the N<sub>2</sub> concentrations (apart from when metallicity is specified and N<sub>2</sub> is set by chemical equilibrium), or the tropospheric relative humidity, which is kept at 1. This is because W24 described how their uninhabited Hycean scenario result was insensitive to these specified parameters. In addition, the inhabited case is consistent over a variety of parameters, because it just requires tuning the CH<sub>4</sub> surface-to-atmosphere flux to get a specific CH<sub>4</sub> mixing ratio. Should K2-18 b be a Hycean exoplanet, given the potential large volume and surface coverage of an ocean relative to the Earth’s ocean (Rigby & Madhusudhan 2024), higher CH<sub>4</sub> fluxes than those present on Earth could be possible, so this is not unfounded in the inhabited Hycean scenarios.

For the mini-Neptune cases using the W24 setup, we vary metallicity between 30 – 200× solar metallicity, the stellar spectrum, the cross section source, the cross section resolution with wavelength, the planetary internal temperature, and the C/O ratio between 0.5 – 2× solar. For a small number of cases shown in Fig. 3, we varied the Bond albedo.

**Table A1.** The boundary conditions and inputs for simulations that used the W24 setup are shown. This includes the volume mixing ratios and fluxes of species at the lower boundary, the initial metallicity, the vertical deposition of various chemical species, the eddy diffusion parameter ( $K_{zz}$ ), the cross section ( $\sigma_\lambda$ ) source, the resolution of the cross section source (native or binned), the stellar input spectrum, and the top of atmosphere albedo. Text in bold are the original parameters that were included in the final simulation results shown in W24, and we note that W24 did test a wider range of parameters than the ones they presented.

Parameter	Uninhabited Hycean	Inhabited Hycean	Mini-Neptune
H <sub>2</sub> O humidity	<b>1.0</b>	<b>1.0</b>	<b>1.0</b>
N <sub>2</sub> mixing ratio	<b><math>3 \times 10^{-3}</math></b>	<b><math>3 \times 10^{-3}</math></b>	<b>See metallicity</b>
CO <sub>2</sub> mixing ratio	<b><math>8 \times 10^{-3}</math></b>	<b><math>8 \times 10^{-3}</math></b>	<b>See metallicity</b>
CH <sub>4</sub> flux [cm <sup>-2</sup> s <sup>-1</sup> ]	–	<b><math>5 \times 10^{10}</math></b>	–
CO $v_{\text{dep}}$ [cm s <sup>-1</sup> ]	–	<b><math>1.2 \times 10^{-4}</math></b>	–
HCCCN $v_{\text{dep}}$ [cm s <sup>-1</sup> ]	<b><math>7 \times 10^{-3}</math></b>	<b><math>7 \times 10^{-3}</math></b>	<b><math>K_{zz}/H</math></b>
HCN $v_{\text{dep}}$ [cm s <sup>-1</sup> ]	<b><math>7 \times 10^{-3}</math></b>	<b><math>7 \times 10^{-3}</math></b>	–
NH <sub>3</sub> $v_{\text{dep}}$ [cm s <sup>-1</sup> ]	–	–	–
C <sub>2</sub> H <sub>6</sub> $v_{\text{dep}}$ [cm s <sup>-1</sup> ]	<b><math>10^{-5}</math></b>	<b><math>10^{-5}</math></b>	<b><math>K_{zz}/H</math></b>
Metallicity (× solar)	–	–	30, 50, <b>100</b> , 200
C/O ratio (× solar) (× solar)	–	–	0.5, <b>1.0</b> , 2.0
$T_{\text{int}}$ [K]	–	–	30, 40, 50, <b>60</b> , 70
$K_{zz}$ [cm <sup>2</sup> s <sup>-1</sup> ]	<b><math>5 \times 10^5</math></b>	<b><math>5 \times 10^5</math></b>	<b>See W24 figure A1b</b>
$\sigma_\lambda$ source (resolution)	<b>Photochem</b> (N), VULCAN (N, B), Atmos (N, B)		
Stellar spectrum	<b>GJ 176</b> , GJ 436, GJ 849		
Top of atmosphere albedo	<b>0.3</b>	<b>0.3</b>	<b>0.0</b> , 0.3, 0.4
Model equilibrium time	<b><math>10^{14}</math> s</b>	<b><math>10^{15}</math> s</b>	<b><math>10^{10}</math> s</b>



**Table A2.** Photochemical simulations performed with VULCAN for K2-18 b. All simulations used either the “SNCHO\_photo\_network\_2024.txt” or the “NCHO\_photo\_network.txt” chemical network. The network without sulfur was used in the Hycean cases, and with sulfur in the mini-Neptune cases, unless otherwise specified in the caption/legend of the figure. Simulations were performed with GJ 176 for the 1 bar Hycean cases, and with a 0.3 top of atmosphere albedo, as used in W24. At higher pressures, we used GJ 436. Cases either start with an initial CH<sub>4</sub> mixing ratio ( $f_{\text{CH}_4}$ ) which is specified arbitrarily, or a CH<sub>4</sub> mixing ratio resulting from initial chemical equilibrium conditions set by the metallicity and the  $P$ - $T$  profile, which was the same as the one used in the W24 Hycean cases for 1 bar. At higher pressures, we used the PT3 profile from Madhusudhan et al. (2023a). The mixing ratio of ( $f_{\text{CO}_2}$ ) is fixed at the lower boundary at the value specified. All simulations use a deposition velocity at the lower boundary to simulate NH<sub>3</sub> dissolving in an ocean, and the dry deposition of HCN, C<sub>2</sub>H<sub>6</sub>, and in the inhabited Hycean case only, CO. Text in bold are the original parameters that were included in the final simulation results shown in W24.

Parameter	Uninhabited Hycean	Inhabited Hycean	Mini-Neptune
H <sub>2</sub> O humidity	0.5, <b>1.0</b>	<b>1.0</b>	<b>1.0</b>
N <sub>2</sub> mixing ratio	<b><math>3 \times 10^{-3}</math></b>	<b><math>3 \times 10^{-3}</math></b>	<b>See metallicity</b>
CO <sub>2</sub> mixing ratio	$1, 2 \times 10^{-3}$ , <b><math>8 \times 10^{-3}</math></b>	<b><math>8 \times 10^{-3}</math></b>	<b>See metallicity</b>
CH <sub>4</sub> flux [cm <sup>-2</sup> s <sup>-1</sup> ]	–	$8 \times 10^{10}$	–
CO $v_{\text{dep}}$ [cm s <sup>-1</sup> ]	–	<b><math>1.2 \times 10^{-4}</math></b>	–
HCCCN $v_{\text{dep}}$ [cm s <sup>-1</sup> ]	<b><math>7 \times 10^{-3}</math></b>	<b><math>7 \times 10^{-3}</math></b>	<b>K<sub>zz</sub>/H</b>
HCN $v_{\text{dep}}$ [cm s <sup>-1</sup> ]	<b><math>7 \times 10^{-3}</math></b>	<b><math>7 \times 10^{-3}</math></b>	–
NH <sub>3</sub> $v_{\text{dep}}$ [cm s <sup>-1</sup> ]	–	–	–
C <sub>2</sub> H <sub>6</sub> $v_{\text{dep}}$ [cm s <sup>-1</sup> ]	<b><math>10^{-5}</math></b>	<b><math>10^{-5}</math></b>	<b>K<sub>zz</sub>/H</b>
Metallicity (× solar)	100–200	–	50, <b>100</b> , 200
C/O ratio (× solar)	1.0	–	<b>1.0</b>
$T_{\text{int}}$ [K]	–	–	<b>60</b>
$K_{\text{zz}}$ [cm <sup>2</sup> s <sup>-1</sup> ]	<b><math>5 \times 10^5</math></b>	<b><math>5 \times 10^5</math></b>	<b>See W24 figure A1b</b>
$\sigma_{\lambda}$ source (resolution)		VULCAN (N)	
Stellar spectrum		<b>GJ 176, GJ 436</b>	
Top of atmosphere albedo	<b>0.3</b>	<b>0.3</b>	<b>0.0</b>
Model equilibrium time	<b><math>10^{17}</math> s</b>	<b><math>10^{17}</math> s</b>	Steady state criterion

We perform only one VULCAN inhabited Hycean simulation to show that the model is consistent with all five abundance constraints. In the VULCAN uninhabited Hycean simulations, we vary initial metallicity, the stellar spectrum, the photodissociation albedo (not the Bond albedo), and the surface pressure. We also tested two photochemical networks.

## B. CROSS SECTIONS AND BRANCHING RATIOS

Photodissociation cross sections and their branching ratios form part of the critical input data for photochemical models. They are crucial for robust calculations of radiative transfer and chemical reactions in planetary atmospheres. We further describe the cross section and branching ratios present in the three models we sourced cross sections from.

Photochem cross section citations are available in a metadata.yaml file<sup>8</sup>, but the original source of many of these cross sections are unknown. The majority of the VULCAN cross sections come from the Leiden database<sup>9</sup>, with a few others sourced from the PhiDrates<sup>10</sup> or MPI-Mainz UV/VIS Spectral Atlas<sup>11</sup> databases. Cross sections references for Atmos come from a variety of sources and some of those sources are given in the relevant folders on GitHub<sup>12</sup>. These include MPI-Mainz, JPL recommendations, and some from unknown sources.

We noticed that the photodissociation cross sections ( $\sigma_{\lambda}$ ) for several species in Photochem do not closely match up-to-date measurements. We found that the data for important atmospheric molecules, such as NH<sub>3</sub>, CO, CO<sub>2</sub>, CH<sub>4</sub>, H<sub>2</sub>O, and H<sub>2</sub>, had significant differences. These are all shown in Fig. B1, alongside the cross sections for HO<sub>2</sub>, HCN,

<sup>8</sup> Photochem github cross section metadata.yaml

<sup>9</sup> <http://home.strw.leidenuniv.nl/~ewine/photo>

<sup>10</sup> <https://phidrates.space.swri.edu/>

<sup>11</sup> <https://www.uv-vis-spectral-atlas-mainz.org/uvvis/>

<sup>12</sup> Atmos Github cross section folder

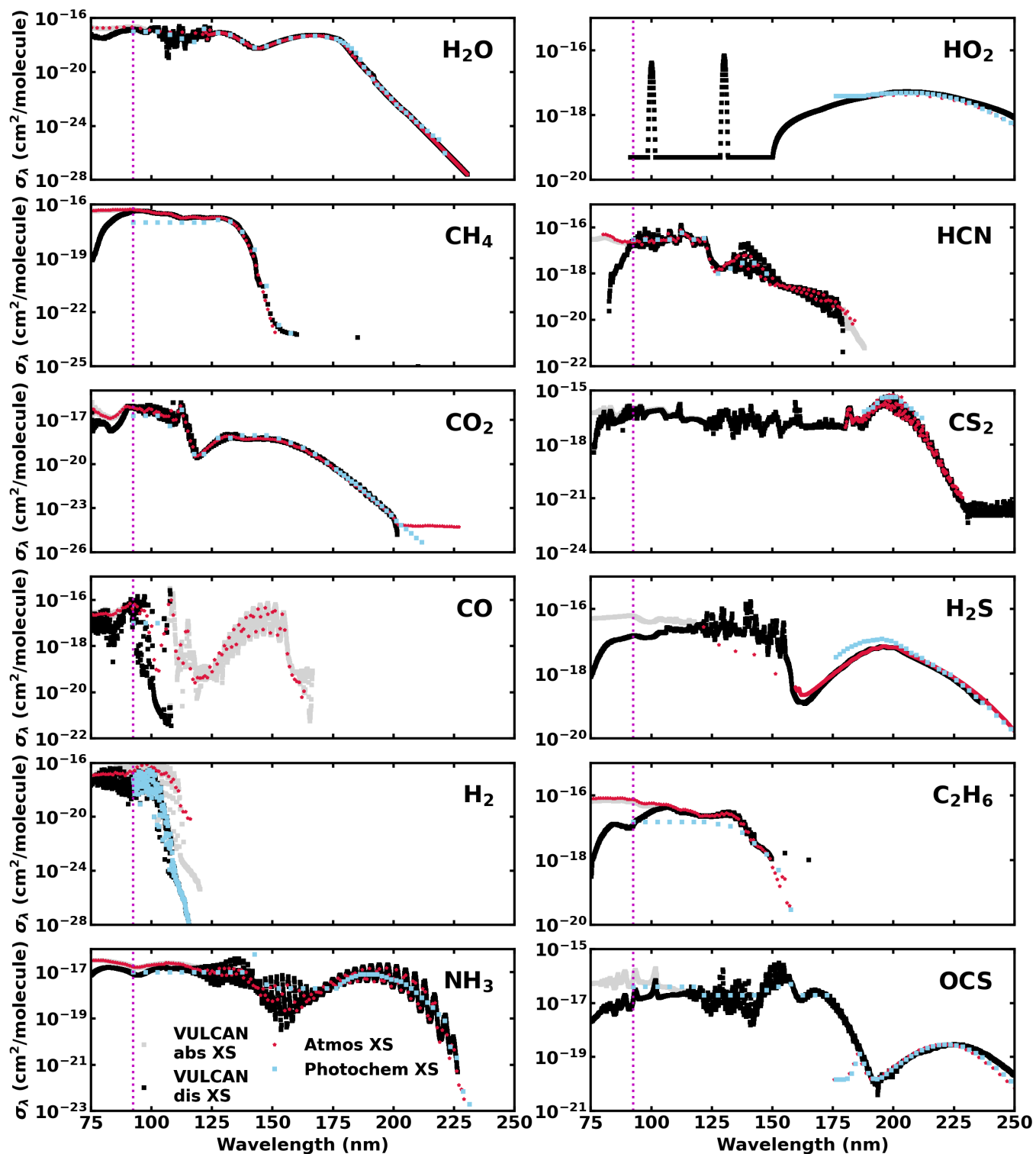


**Figure B1.** Photodissociation cross sections for twelve molecules are compared across three models. Cross sections ( $\sigma_\lambda$ ) in terms of  $\text{cm}^2 \text{ molecule}^{-1}$  are shown for  $\text{H}_2\text{O}$ ,  $\text{CH}_4$ ,  $\text{H}_2$ ,  $\text{CO}$ ,  $\text{CO}_2$ ,  $\text{NH}_3$  in the left column on a log scale and the right column shows the cross section for  $\text{HO}_2$ ,  $\text{HCN}$ ,  $\text{CS}_2$ ,  $\text{H}_2\text{S}$ ,  $\text{C}_2\text{H}_6$ , and  $\text{OCS}$  and linear (right) scale versus wavelength in nm. Available cross sections in Atmos and Photochem are shown in red and light blue, respectively. VULCAN has cross sections given in terms of absorption (grey) and dissociation (black). The vertical magenta dotted line shows where the Photochem photolysis grid starts at 92.5 nm.

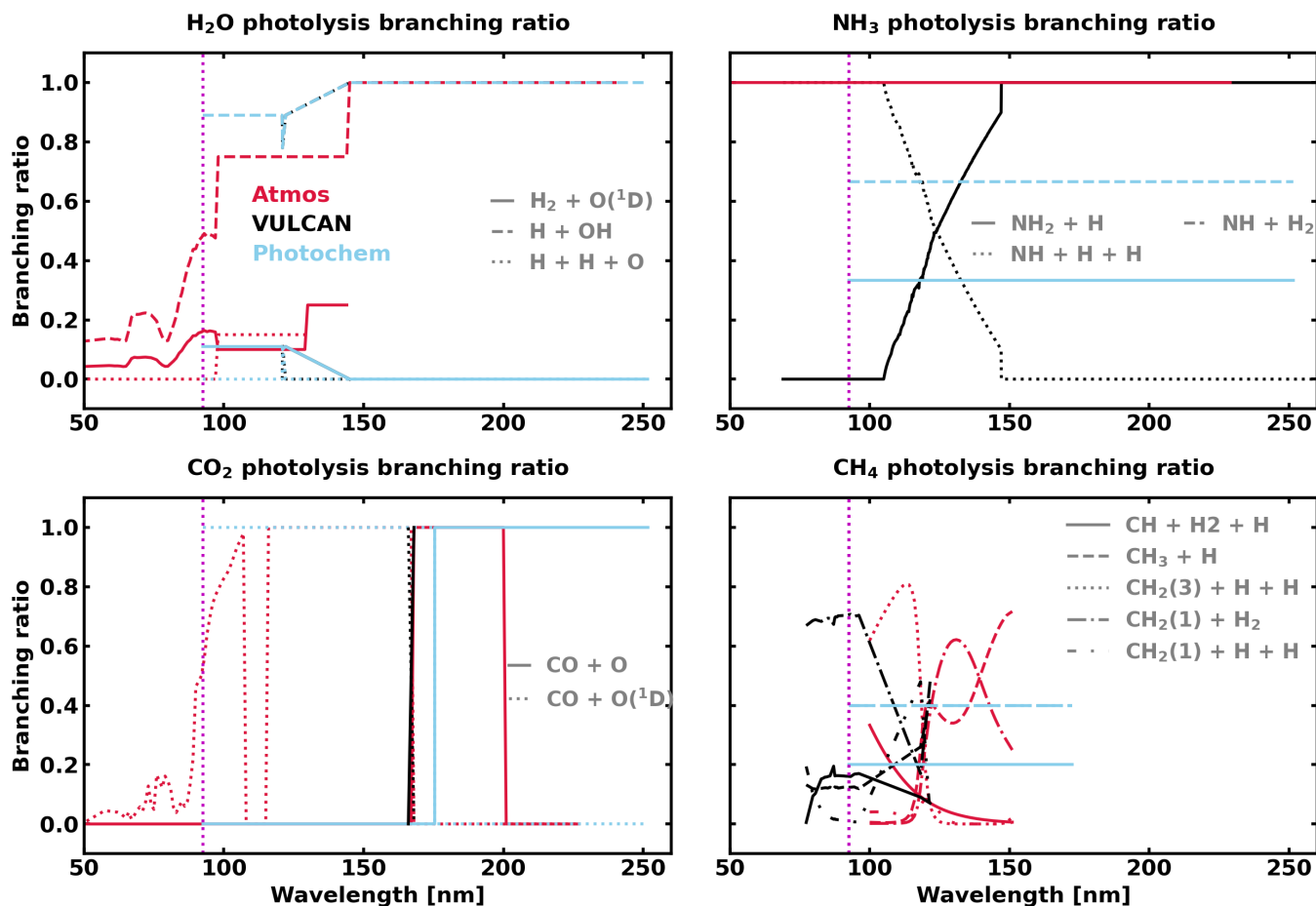


**Figure B2.** Branching ratios for four molecules compared between three models. Photolysis channels and their respective branching ratios are shown for  $\text{H}_2\text{O}$ ,  $\text{NH}_3$ ,  $\text{CO}_2$ ,  $\text{CH}_4$  versus wavelength in nm. The data are taken from VULCAN, Atmos, and Photochem, and are shown in black, red, and light blue, respectively.  $\text{H}_2\text{O}$  branching ratio data between Photochem and VULCAN match, but differ for Atmos. The data for the three other molecules does not match. Additionally, not all three models consider the same photolysis channels.

$\text{CS}_2$ ,  $\text{H}_2\text{S}$ ,  $\text{C}_2\text{H}_6$ , and  $\text{OCS}$ . Depending on whether the VULCAN photoabsorption or photodissociation cross sections are considered, the data may show similarities or discrepancies with the Atmos cross sections.

We now describe a few important molecules and how their cross sections vary between models. The  $\text{H}_2\text{O}$  cross section data is very similar between all three models from 125 – 220 nm. However, longward of 221 nm, it appears that the  $\text{H}_2\text{O}$  cross sections have not been extended in Photochem as recommended by [Ranjan et al. \(2020\)](#), with these wavelengths important for OH production. Between 92.5 – 127.5 nm,  $\text{CH}_4$  cross sections for Photochem have smaller values compared to the other two models. The  $\text{CH}_4$  cross sections end at 151.0 nm and 157.5 nm in Atmos and Photochem, respectively, but continue in VULCAN until 237.3 nm. All three models significantly diverge for  $\text{CO}_2$  longward of 200 nm and this will affect production rates for CO and O (and also is impacted by the specified  $\text{CO}_2$  mixing ratio) in atmospheric modeling. The  $\sigma_\lambda$  data for CO in Photochem has the same cross section ( $1.00000000\text{e-}17$ ) for three given wavelengths (92.5 nm, 97.5 nm, 102.5 nm), and 0 at all other given wavelengths, whereas Atmos and VULCAN have CO cross sections varying over 5 orders of magnitude between 92 nm and 160 nm.  $\text{H}_2$ , which makes up the majority of these mini-Neptune and Hycean atmospheres, has large cross section differences in magnitude and shape between all three models between 90 and 120 nm. In the case of  $\text{NH}_3$ , between 92.5 - 142.5 nm, all three models have varied  $\sigma_\lambda$  values which do not closely match. After 142.5 nm, differences arise due to the assumed resolution of the data.

Whilst not shown in Fig. B1, the cross sections for  $\text{N}_2$ ,  $\text{N}_2\text{O}$ ,  $\text{NO}_2$ , SO,  $\text{SO}_2$ ,  $\text{C}_2\text{H}_2$ ,  $\text{C}_2\text{H}_4$ ,  $\text{H}_2\text{CO}$ ,  $\text{HNO}_3$ , and  $\text{H}_2\text{O}_2$ , also exhibit large discrepancies between the three models at wavelengths relevant to the Photochem photolysis grid.

This is 22 molecules in total. Discrepancies also exist for  $\text{CH}_2\text{CO}$ ,  $\text{HS}$ ,  $\text{CH}_3\text{CN}$ ,  $\text{CH}_3\text{OH}$ ,  $\text{OH}$ ,  $\text{NO}$ , and  $\text{H}_2\text{SO}_4$ , but these are not available in all three models, so we do not swap these molecules. Furthermore, **Photochem** does not include cross sections for  $\text{CH}_3$ ,  $\text{CH}_2$ , or  $\text{CH}$ , which do undergo photodissociation at UV wavelengths. Note that the resolution of the cross section ( $\sigma_\lambda$ ) data for each model and molecule varies.

We tested simulations where we only swapped 6 ( $\text{NH}_3$ ,  $\text{CO}$ ,  $\text{CO}_2$ ,  $\text{CH}_4$ ,  $\text{H}_2\text{O}$ , and  $\text{H}_2$ ) out of the 22 molecules. The reason for this is that updates to specific sets of molecules, whilst not updating others, can change the predicted results (i.e., three sets of cross sections give three results). Whilst this seems obvious, we explicitly say this because it is factual for multiple models used by the community and for results scattered throughout the literature. We found that significant differences (up to a factor of 10 billion) could occur for important molecules such as  $\text{NH}_3$  in the Hycean scenarios, although this was reduced from an initially small abundance of  $\sim 1$  pptv. Testing every single combination of molecules would require millions of simulations, but we deduced that the main source of the changes in the simulations with only 6 changed molecular cross sections was due to  $\text{CO}$ .

Because the **Atmos** and **Photochem** codes photodissociate at wavelengths where **VULCAN** only considers photoabsorption (e.g, see  $\text{CO}$  in Fig. B1), we implement the **VULCAN** photoabsorption and photodissociation values together when swapping in the photodissociation values used in **Photochem** for the W24 setup sensitivity tests (see section 4.1). One can also only swap photodissociation and leave out the photoabsorption. Either way, due to the discrepancies between the data, incident photons are accounted for in different ways, with some either being allowed to propagate through atmospheric layers they should be absorbed by, or with some photons affecting photochemical reactions when they should not be.

Additionally, molecular photolysis can have multiple photochemical reaction channels, with a branching ratio which represents the likelihood of a photochemical reaction channel occurring at a particular wavelength. We have found that the branching ratios between the three models do not always agree, with discrepancies for  $\text{H}_2\text{O}$ ,  $\text{NH}_3$ ,  $\text{CO}_2$ ,  $\text{CH}_4$ ,  $\text{O}_3$ ,  $\text{SO}_2$ ,  $\text{CH}_3\text{OH}$ ,  $\text{H}_2\text{CO}$ ,  $\text{C}_2\text{H}_4$ , and  $\text{C}_2\text{H}_6$ . We show the differences for  $\text{H}_2\text{O}$ ,  $\text{NH}_3$ ,  $\text{CO}_2$ , and  $\text{CH}_4$  in Fig B2.

To further complicate matters, the photolysis channels assumed are not always the same. For example, the following  $\text{NH}_3$  photolysis channels exist:



**Photochem** uses channels B1 and B3, **VULCAN** uses channels B1 and B2, but **Atmos** uses only channel B1. For  $\text{CH}_4$ , **Photochem** includes 3 channels, **VULCAN** includes 4 channels, and **Atmos** includes 5 channels. In the case of  $\text{C}_2\text{H}_6$ , **Photochem** includes 1 channel, **VULCAN** includes 5 channels, and **Atmos** includes 6 channels. We also found differences in assumed photolysis channels for  $\text{S}_4$ ,  $\text{SO}_2$ ,  $\text{H}_2\text{CO}$ ,  $\text{CH}_3$ ,  $\text{CS}_2$ ,  $\text{C}_2\text{H}_2$ ,  $\text{C}_2\text{H}_4$ , and  $\text{C}_2\text{H}_6$ . Testing all of the differences in cross sections, branching ratios, and photolysis channels is a significant undertaking and our aim is to point out model differences and the possible arising uncertainties.

### C. THE ASSUMED STELLAR SPECTRUM

When there are no spectral measurements in the UV for a particular star, using another star which closely matches the stellar parameters as an analogue is the most reasonable method for estimating the photochemical environment of the exoplanet’s atmosphere. However, the strength and shape of the incoming UV affects molecular photolysis rates, which in turn determines the transmission spectrum that can be retrieved from afar. This is without stellar variability and activity being accounted for, which would further complicate the picture.

Several MUSCLES stars have spectral types which differ depending on the study. According to [Benneke et al. \(2017\)](#), K2-18 is an  $\text{M}2.5 \pm 0.5\text{V}$  star, and [Montet et al. \(2015\)](#) list it as an  $\text{M}2.8\text{V}$ . GJ 176 is listed as an  $\text{M}2.5\text{V}$  star ([von Braun et al. 2014](#); [Forveille et al. 2009](#)) and an  $\text{M}2\text{V}$  star ([Kiraga & Stepien 2007](#)). [Loyd et al. \(2016\)](#) lists GJ 436 as a  $\text{M}3.5\text{V}$  dwarf, whilst [Youngblood et al. \(2017\)](#) lists it as an  $\text{M}3\text{V}$  dwarf, citing [von Braun et al. \(2012\)](#), who cite [Hawley et al. \(1996\)](#) and [Kirkpatrick et al. \(1991\)](#) for this purpose. [Salz et al. \(2015\)](#) give it as an  $\text{M}2.5\text{V}$  star. TOI-270 is listed as an  $\text{M}3\text{V}$  star by [Mikal-Evans et al. \(2023\)](#) and an  $\text{M}3.0 \pm 0.5\text{V}$  star according to [Günther et al. \(2019\)](#). Because of the uncertainty on these stellar measurements and their derived spectral type, the spectral types of GJ 849 ( $\text{M}3\text{V}$ ), GJ 832 ( $\text{M}1.5\text{V}$ ), GJ 674 ( $\text{M}3\text{V}$ ), and GJ 436 ( $\text{M}3.5\text{V}$ ) overlap with K2-18, whilst GJ 436 ( $\text{M}3.5\text{V}$ ), GJ 674 ( $\text{M}3\text{V}$ ), GJ 163 ( $\text{M}3.5\text{V}$ ), GJ 849 ( $\text{M}3.5\text{V}$ ), GJ 729 ( $\text{M}3.5\text{V}$ ), and GJ 176 ( $\text{M}2.5\text{V}$ ) overlap with TOI-270.

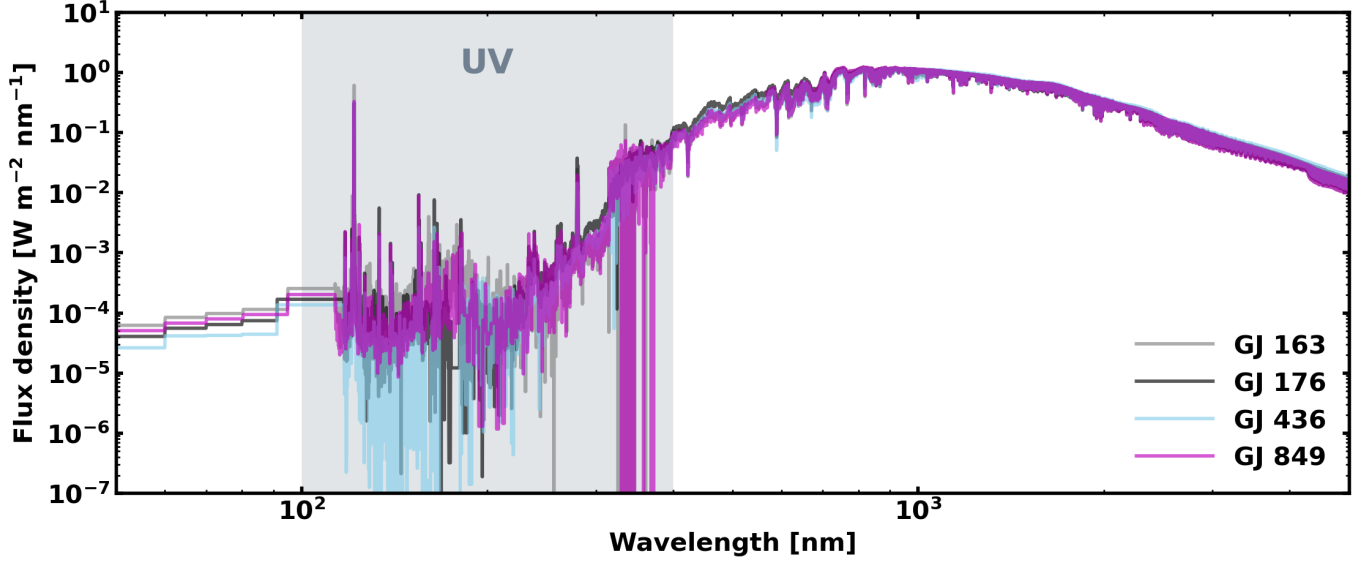


**Figure C1.** Stellar spectra for four M dwarf stars. The flux density of MUSCLES stars versus wavelength in nm are plotted for the following stars: GJ 163 (grey), GJ 176 (black), GJ 436 (light blue), GJ 849 (magenta). The spectra are normalised to the irradiance K2-18 b receives, which is  $1368 \text{ W m}^{-2}$ . These stars are all reported to be between M2.5V and M3.5V, with associated errors in observations (see main text, Fig. C2, and Table C1).

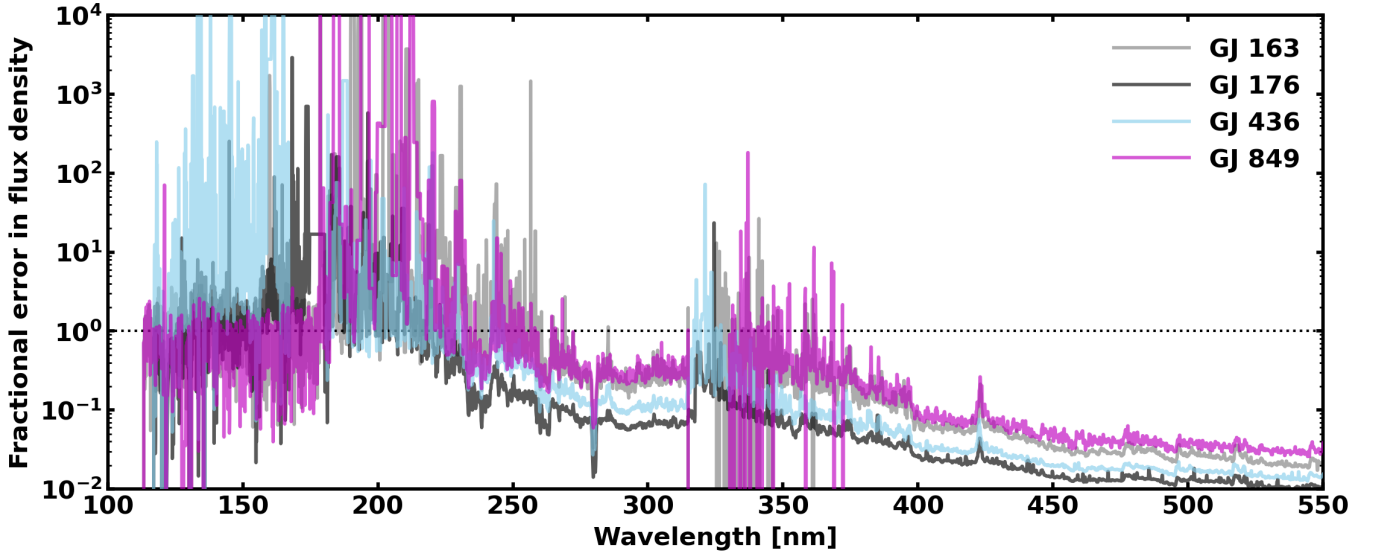


**Figure C2.** The uncertainty in the stellar spectra for four stars at UV/VIS wavelengths. The fractional error in flux density of MUSCLES stars versus wavelength in nm are plotted for the following stars: GJ 163 (grey), GJ 176 (black), GJ 436 (light blue), GJ 849 (magenta). The black dotted line shows where the reported error in flux is equal to the flux.

Stellar effective temperature ( $T_{\text{eff}}$ ), mass, and rotation can be measured from observations but age constraints are more uncertain (Brown et al. 2023). These stellar properties are summarised in Table C1.

Scheucher et al. (2020) used the GJ 176 spectrum in lieu of a well characterised K2-18 UV spectrum, stating that GJ 176 has stellar properties which closely match K2-18. Subsequently, Hu et al. (2021), W24, and Shorttle et al. (2024) have used the GJ 176 spectrum in place of K2-18. For these two stars, the mass, radius and rotation overlap at the  $1\text{-}\sigma$  level, but the stellar effective temperature ( $T_{\text{eff}}$ ) and ages overlap at the  $2\text{-}\sigma$  level, though K2-18 is estimated to be much younger ( $2.4 \pm 0.6$  Gyr old) compared to GJ 176 ( $8.8_{-2.8}^{+2.5}$  Gyr old). Tsai et al. (2024a) recently simulated K2-18 b and varied the stellar spectrum, using GJ 436 (listing it as an M2.5V star) as the closest match to K2-18.

**Table C1.** Several different stellar spectra are considered in this study. The spectral type, mass, radius, effective temperature, age, and rotation rate of different stars with associated errors are listed. The relevant references are given here: **(a)** Benneke et al. (2017); Montet et al. (2015); Sarkis et al. (2018); Guinan & Engle (2019) **(b)** Mikal-Evans et al. (2023); Günther et al. (2019); Van Eylen et al. (2021) **(c)** Pineda et al. (2021a); Tuomi & Anglada-Escudé (2013); Suárez Mascareño et al. (2015) **(d)** von Braun et al. (2014); Forveille et al. (2009); Kiraga & Stepien (2007); Pineda et al. (2021a); Forveille et al. (2009) **(e)** Bourrier et al. (2018); Loyd et al. (2016); Youngblood et al. (2017); von Braun et al. (2012); Hawley et al. (1996); Kirkpatrick et al. (1991); Salz et al. (2015) **(f)** Hawley et al. (1996); Bonfils et al. (2007); Froning et al. (2019); Linsky et al. (2020); Brown et al. (2023); Pineda et al. (2021a); Suárez Mascareño et al. (2015) **(g)** Pineda et al. (2021a); Ibañez Bustos et al. (2020) **(h)** Bonfils et al. (2013); Pineda et al. (2021a); Pinamonti et al. (2023); Butler et al. (2006); Brown et al. (2023) **(i)** Correia et al. (2010); Pineda et al. (2021a); Moutou et al. (2023); Loyd et al. (2016). It is noted that some of the references used list different values for some of the parameters that we list here. This gives added uncertainty to what stellar proxy can be assumed for a particular star and planet.

Star	UV measured?	Spec type	Mass [ $M_{\odot}$ ]	Radius [ $R_{\odot}$ ]	$T_{\text{eff}}$ [K]	Age [Gyr]	Rotation [d]	References
K2-18	No	$M2.5 \pm 0.5V$	$0.4951 \pm 0.0043$	$0.4445 \pm 0.0148$	$3457 \pm 39$	$2.4 \pm 0.6$	$39.6 \pm 0.50$	a
TOI-270	No	$M3.0 \pm 0.5V$	$0.386 \pm 0.008$	$0.378 \pm 0.011$	$3506 \pm 70$	–	$\sim 58$	b
GJ 163	Yes	$M3.5V$	$0.405 \pm 0.010$	$0.409^{+0.017}_{-0.016}$	$3460^{+76}_{-74}$	1 – 10	$61.0 \pm 0.3$ d	c
GJ 176	Yes	$M2V$ or $M2.5V$	$0.485 \pm 0.012$	$0.474 \pm 0.015$	$3632^{+56}_{-58}$	$8.8^{+2.5}_{-2.8}$	$40.00 \pm 0.11$	d
GJ 436	Yes	$M3 \pm 0.5V$	$0.445 \pm 0.044$	$0.449 \pm 0.019$	$3479 \pm 60$	$8.9^{+2.3}_{-2.1}$	$44.09 \pm 0.08$	e
GJ 674	Yes	$M2.5V$ or $M3V$	$0.353 \pm 0.008$	$0.361^{+0.011}_{-0.012}$	$3404^{+57}_{-59}$	0.20	$32.9 \pm 0.1$	f
GJ 729	Yes	$M3.5V$	$0.177 \pm 0.004$	$0.200 \pm 0.008$	$3248^{+68}_{-66}$	$0.7^{+0.5}_{-0.3}$	$2.848 \pm 0.001$	g
GJ 849	Yes	$M3V$ or $M3.5V$	$0.465 \pm 0.011$	$0.464 \pm 0.018$	$3492^{+70}_{-68}$	$4.9^{+3.0}_{-2.1}$	$40.45^{+0.19}_{-0.18}$	h
GJ 876	Yes	$M4V$ or $M5V$	$0.346 \pm 0.007$	$0.372 \pm 0.004$	$3201^{+20}_{-19}$	0.1 – 9.9	$83.7 \pm 2.9$	i

GJ 436 is a good match for most parameters in Table C1, apart from for the age and rotation rate. Yang & Hu (2024a), who modelled K2-18 b and TOI-270 d as a mini-Neptune, use the M4V – M5V star GJ 876 to approximate K2-18. These stars only overlap for age and radius. The mass,  $T_{\text{eff}}$  and rotation overlap at  $3\text{-}\sigma$  or worse, such that GJ 876 is not a good proxy for K2-18.

We now consider the properties of GJ 849. For K2-18 and GJ 849, the radius,  $T_{\text{eff}}$ , and age overlap at the  $1\text{-}\sigma$  level, while the rotation and mass overlap at the  $2\text{-}\sigma$  level. Both age and rotation rate influence an M dwarf star’s UV emission and activity level (Loyd et al. 2021; Pineda et al. 2021b). Hence, one could assume that K2-18 can be approximated by GJ 849 instead of GJ 176 or GJ 436.

Benneke et al. (2024) also used GJ 176 in place of TOI-270. These two stars overlap at the  $1\text{-}\sigma$  level for  $T_{\text{eff}}$ , but their masses, radii, and rotation do not overlap at the  $3\text{-}\sigma$  level so these parameters are inconsistent. Again, we consider the properties of a different star. It seems that GJ 163 is the best match to TOI-270 for the stars in Table C1 when considering mass,  $T_{\text{eff}}$ , and rotation.

Fig. C1 shows the MUSCLES stellar spectra of GJ 163, GJ 176, GJ 436, and GJ 849, with the UV wavelengths highlighted between 100 – 400 nm. These spectra are given with uncertainties: the fractional uncertainty in flux density for these stars is shown in Fig. C2. This fractional uncertainty can be very large (up to 10,000) and frequently exceeds 1 for several stars between 100 – 350 nm.